The Behavior of $O-C$ Curves for Contact Binaries in the *Kepler* Catalog

by

Kathy Tran

Submitted to the Department of Physics
in partial fulfillment of the requirements for the degree of

Bachelor of Science in Physics

at the

MASSACHUSETTS INSTITUTE OF TECHNOLOGY

June 2013

Author .....
Department of Physics
May 17, 2013

Certified by.....
Saul A. Rappaport
Professor Emeritus
Thesis Supervisor

Accepted by .....
Nergis Mavalvala
Thesis Coordinator

The Behavior of $O - C$ Curves for Contact Binaries in the *Kepler* Catalog

by

Kathy Tran

Submitted to the Department of Physics
on May 17, 2013, in partial fulfillment of the
requirements for the degree of
Bachelor of Science in Physics

Abstract

In this thesis, we study the timing of eclipses for contact binary systems in the *Kepler* catalog. Observed eclipse times were determined from *Kepler* long-cadence light curves and "observed minus calculated" ($O - C$) curves were generated for both primary and secondary eclipses of the contact binary systems. We found the $O - C$ curves of contact binaries to be clearly distinctive from the curves of other binaries. The key characteristics of these curves are random-walk like variations, with typical semi-amplitudes of 200 to 300 seconds, quasi-periodicities, and anti-correlated behavior between the curves of the primary and secondary eclipses. We performed a formal analysis of systems with dominant anti-correlated behavior, calculating correlation coefficients as low as -0.77, with a mean value of -0.42. We dismiss several physical explanations to account for the observed the anti-correlation of the $O - C$ curves. Instead, we propose a simple geometric model of a starspot that is continuously visible around the orbit.

Thesis Supervisor: Saul A. Rappaport
Title: Professor Emeritus

Acknowledgments

We would like to thank the *Kepler* Eclipsing Binary Team for generating the catalog of eclipsing binaries used in this work. In addition, we are grateful to Roberto Sanchis-Ojeda for his help in preparing the stitched data sets. We thank Prof. Tamas Borkovits, Dr. Szilard Csizmadia, Prof. Belinda Kalomeni, Dr. Alan Levine, and Prof. Saul Rappaport for all their work and collaborative effort in the research of this thesis topic. In particular, the author extends her deepest gratitude to Dr. Alan Levine and Prof. Saul Rappaport for their patient guidance and generous support.

Contents

List of Figures

List of Tables

Chapter 1

Introduction

1.1 Binary Stars

A binary system consists of two gravitionally bound stars orbiting around their common center of mass. The brighter and/or more massive star is typically called the *primary*, while its companion is called the *secondary*. The period, P, of the orbital motion of the binary star system is given by Kepler's Third Law,

$$(\frac{P}{2\pi})^2 = \frac{a^3}{G(m_1 + m_2)} \tag{1.1}$$

where G is the gravitational constant, m_1 and m_2 are the masses of each star, and a is semi-major axis describing the full separation between the two stars. The effective gravitational potential of a binary system, in the frame of reference that rotates with the orbital period, is described by the Roche potential. If the two masses are located along the x-axis at the positions $x_1 = -am_1/(m_1 + m_2)$ and $x_2 = am_2/(m_1 + m_2)$, this potential is represented by the following expression

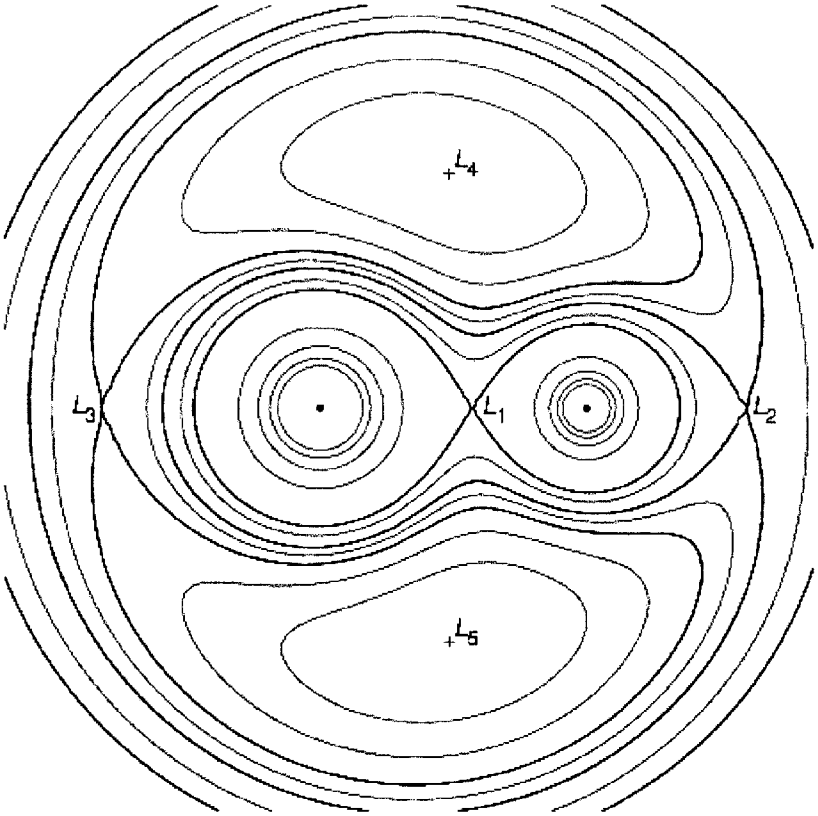

Figure 1-1: An illustrative contour plot of the Roche potential of a binary system with a mass ratio of 2 to 1, with the location of the Lagrangian points labeled, taken from Bhattacharyya (2009). The equipotential surface containing the point L_1 defines the Roche lobes of each star.

$$\Psi(x,y,z) = \Psi_0\Big[\frac{q}{(1+q)\sqrt{(x-x_1)^2+y^2+z^2}} - \frac{1}{(1+q)\sqrt{(x-x_2)^2+y^2+z^2}} - \frac{x^2+y^2}{2}\Big] \tag{1.2}$$

where Ψ_0 is a constant associated with a particular binary system, x, y, and z are dimensionless lengths, and q is the mass ratio m_1/m_2. An illustrative contour plot of the Roche potential of an example binary system with a 2 to 1 mass ratio is shown in Figure 1-1.

The Roche lobe defines a region of space around a star in a binary system within which material can be bound in hydrostatic equilibrium. The gradient of the po-

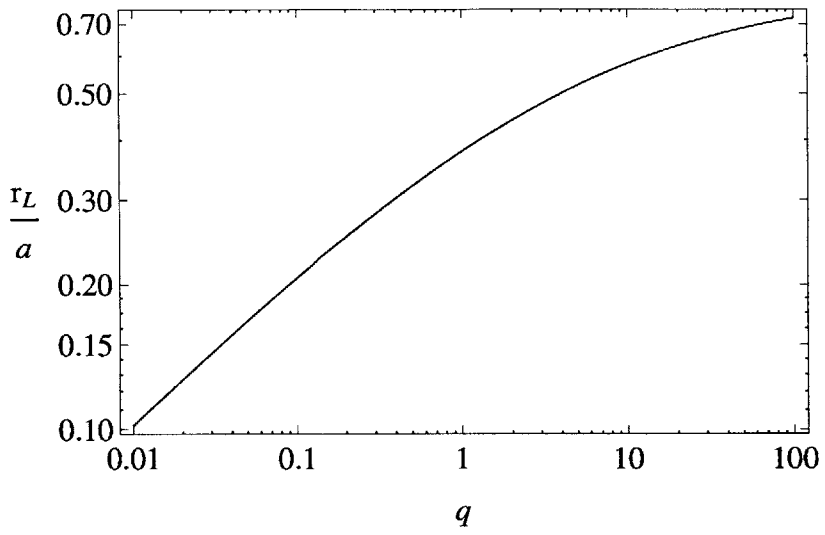

Figure 1-2: The Roche lobe radius r_L of a star in a binary system, divided by the semi-major axis a of the two stars, plotted against the mass ratio q on a log-log scale.

tential everywhere is pointed inward along the Roche lobe, except exactly at the L_1 Langragian point. Within the Roche lobe the inward force associated with $-\vec{\nabla}\Psi$ can be balanced by pressure gradients in the fluid. If the matter of a star fills or overfills its Roche lobe, then it will be forced to flow through L_1 towards the other star. The radius of the Roche lobe is defined as the radius of a sphere with the same volume as the Roche lobe. This volume equivalent radius of the Roche lobe of a star is given by Eggleton (1983) as

$$r_L = \frac{0.49q^{2/3}}{0.6q^{2/3} + ln(1 + q^{1/3})}, 0 < q < \infty \tag{1.3}$$

A plot of the effective radius of the Roche lobe as a function of q is shown in Figure 1-2.

In the case that the observer lies in, or close to, the orbital plane of the binary system, each star will periodically eclipse the other, blocking at least some of the light from the other star. Such binary systems are known as *eclipsing binaries.* They can be detected by making photometric observations and measuring the periodic variations in their brightness due to these occultations. Such observations can be

used to produce orbital light curves, from which it is possible to determine a number of physical parameters of the binary and of its constituent stars, including stellar mass and radius. Therefore, the study of eclipsing binaries provides a very important tool for the field of stellar astrophysics.

Binary systems can be furthered classified according to their properties, largely based on the orbital separation of the components. Using the designations from the Prša et. al (2011) catalog, these types are denoted detached (D), semi-detached (SD), overcontact (OC), and ellipsoidal light variations (ELV).

1.1.1 Detached Binaries

A detached (D) binary system consists of stars which are contained within their Roche lobes. In other words, the radius of each star is less than the radius of its Roche lobe. Therefore, the components of detached binaries do not undergo any substantial processes of mass transfer, especially via Roche-lobe overflow. Most binaries are detached systems.

Detached binaries can be widely-spaced stars, that is to say, the separation of the stars is typically large relative to their radii. Because of this type of configuration, the duration of eclipses of these systems is relatively short compared to the orbital period of the binary. As a result, the light curves of a detached binary are characterized by sharp, narrow dips, corresponding to the eclipses, and relatively flat, well-defined out-of-eclipse regions. A set of folded light curves for two example detached systems is shown in Figure 1-3.

1.1.2 Semi-Detached Binaries

A semi-detached (SD) binary system is a binary in which one of the component stars fills its Roche lobe while the other does not. The material of a star that expands past its Roche lobe can escape the gravitational pull of that star and will likely flow onto the companion. Therefore, mass transfer can occur in these semi-detached systems. In that case, the star which has filled its Roche lobe will contribute material to an

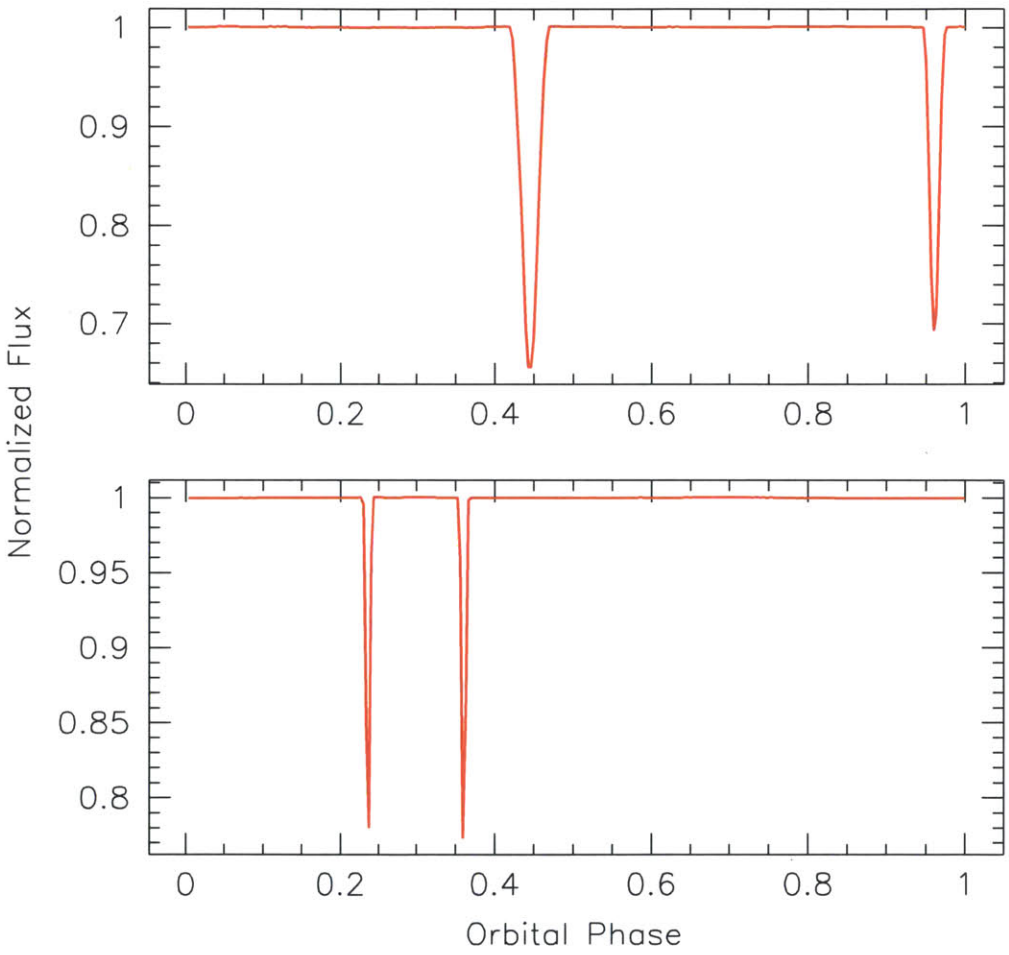

Figure 1-3: Two folded light curves of example detached (D) binary systems, KIC 2306740 and KIC 6864859. The key features of light curves for detached binaries are the sharp, narrow eclipses and flat, well-defined out-of-eclipse regions. It is also interesting to note the unequal eclipse spacing of the second light curve, due to the fact that the system in the bottom panel is a long period eccentric binary.

accretion disk around the other star.

Compared to completely detached systems, the separation between the components of a semi-detached binary relative to their radii is smaller and, therefore, the duration of eclipses relative to the orbital period, is longer. As a result, the light curves of these semi-detached systems have wide, but still well-defined eclipses. In addition, the out-of-eclipse regions tend to be rounded rather than flat, due to the effects of tidal deformations of the surfaces of one or both stars caused by the other. These are called *ellipsoidal light variations*. A set of folded light curves for two example semi-detached binary systems is shown in Figure 1-4.

1.1.3 Contact Binaries

An overcontact (OC), or contact, binary system has stellar components which both fill or slightly overfill their Roche lobes. As a result, the components of the binary are surrounded by a low-density common envelope (Wilson 1994). The properties of the shared convective envelope and the mass and energy transfer that occur via this envelope have been investigated by numerous authors (Kähler 2002; Webbink 2003; Kähler 2004; Csizmadia & Klagyivik 2004; Li et al. 2004; Yakut & Eggleton 2005; Stepień & Gazeas 2012). This thesis will focus particularly on the study of this type of binary system.

The separation between the components of a contact binary relative to their radii, by definition, is very small. Most systems, though not all, have orbital periods between 0.2 and 1.0 days (Maceroni & van't Veer 1996; Paczyński et al. 2006). Contact binaries exhibit constantly changing flux, making features of their light curves less well-defined compared to those of detached and semi-detached binaries. The light curves of contact binaries typically have a nearly sinusoidal shape, with wide eclipses and no well-defined out-of-eclipse regions. A set of folded light curves for two illustrative contact binary systems is shown in Figure 1-5.

Contact binaries occur relatively frequently (Rucinski 1998) among the class of eclipsing binaries and make up an important part of the galactic stellar population. However, the nature of their formation and final evolutionary states is still not entirely

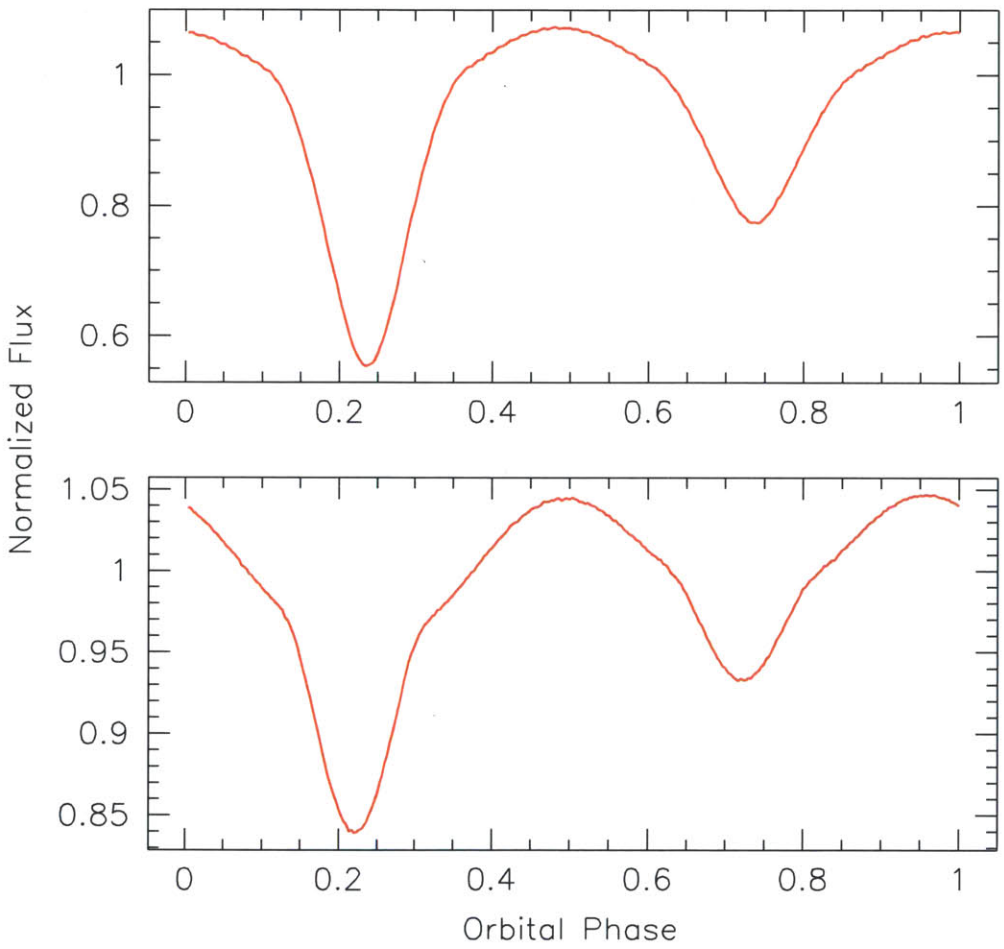

Figure 1-4: Two folded light curves of illustrative semi-detached (SD) binaries, KIC 3228863 and KIC 6865626. The light curves for semi-detached binaries are characterized by wide, but well-defined eclipses and rounded out-of-eclipse regions.

clear (Paczyński et al. 2006; Eggleton 2006). Many contact binaries may be part of systems with a third star, whose presence may drive their formation through a combination of the Kozai mechanism and tidal friction (Robertson & Eggleton 1977; Kozai 1962; Kiseleva et al. 1998; Fabrycky & Tremaine 2007). It is also thought that the components of contact binaries may eventually merge and form rapidly rotating single stars (Li et al. 2008; Gazeas & Stepień 2008).

Many contact binaries show several signs of vigorous stellar activity, likely due to the rapid rotation of the stars if they are tidally locked with the orbit. Doppler imaging has revealed that some contact binaries are almost fully covered by rather chaotic starspot structures (Maceroni et al. 1994 on AE Phe and YY Eri; Hendry & Mochnacki 2000 on VW Cep; Barnes et al. 2004 on AE Phe; Senavci et al. on SW Lac).

1.1.4 Ellipsoidal Light Variation Binaries

Ellipsoidal Light Variation (ELV) binaries are close binary systems that exhibit periodic light variations due to their mutual tidal distortions, but no actual eclipses. Due to the inclination of the orbital plane of these systems, eclipses are not quite observable (see Equation (4.12) for the condition on the inclination angle in order to observe an eclipse). However, because the components of the binary are so close together, they can tidally distort each other, causing detectable changes in brightness, i.e., ellipsoidal light variations. As a result, their light curves have no identifiable eclipses and display nearly sinusoidal behavior. A set of folded light curves for two illustrative ELV systems is shown in Figure 1-6.

1.2 $O-C$ Curves

A very useful tool for analyzing these systems of eclipsing binaries are "observed minus calculated" ($O-C$) curves. Such curves show the delay in the observed times of eclipses compared to the expected, or calculated, time, based on an assumed constant orbital period. The shape of the $O-C$ curve can reveal a number of features. For

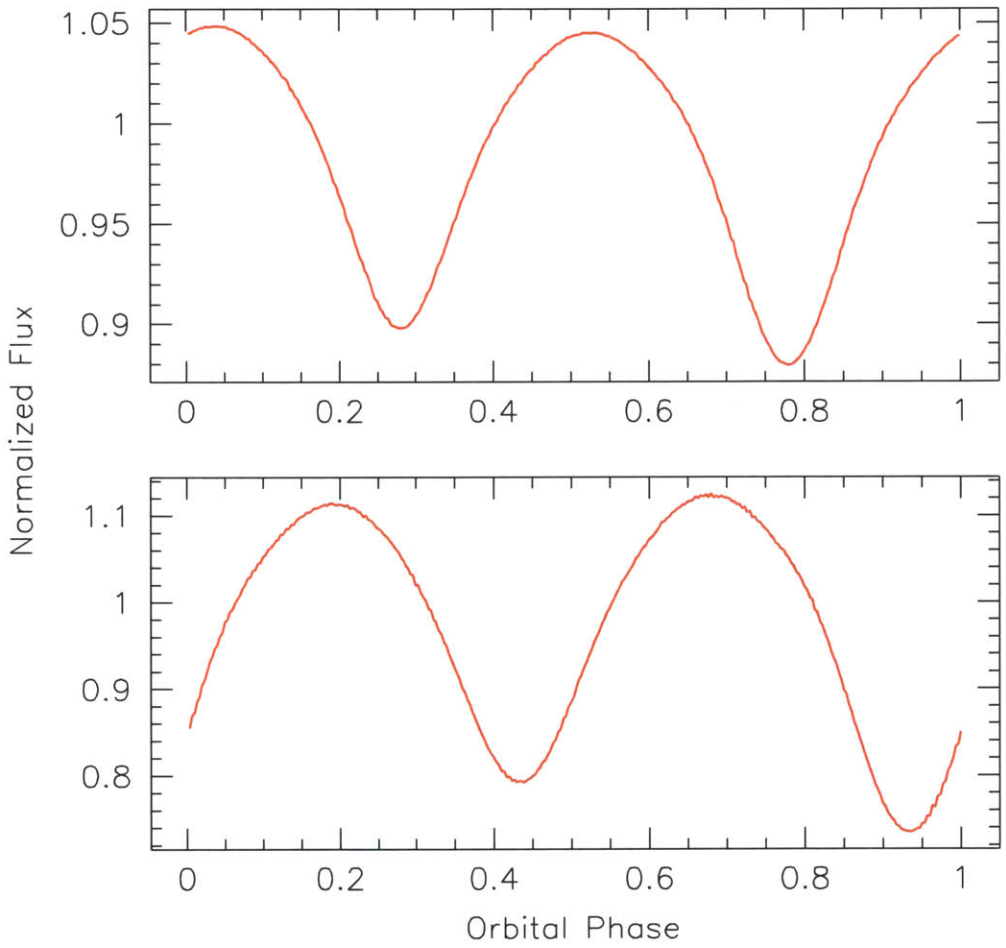

Figure 1-5: Two folded light curves of example overcontact (OC), or contact, binaries, KIC 4074532 and KIC 6106771. The light curves for contact binary systems do exhibit eclipses, which sometimes have clearly different depths, such as the system in the bottom panel. However,the out-of-eclipse regions of the light curves are not well-defined and the over-all characteristic shape of the curves can be nearly sinusoidal.

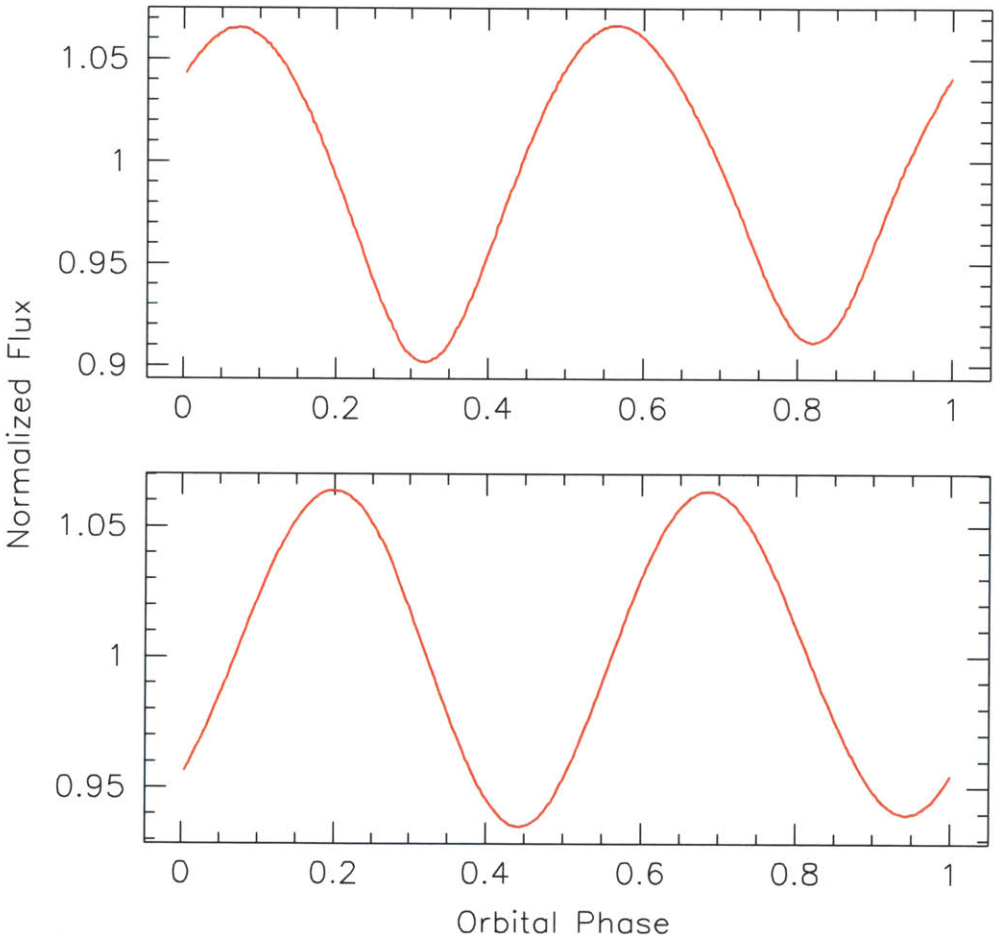

Figure 1-6: Two folded light curves of example ellipsoidal (ELV) binaries, KIC 6067735 and KIC 10481912. The light curves of ellipsoidal system exhibit nearly sinusoidal variations and no detectable eclipses. The intensity modulations are due entirely to the mutual tidal distortions of the stars.

example, a straight line with zero slope indicates that the assumed orbital period used to calculate the curve is accurate. If the assumed orbital period is slightly off from the actual value, the $O - C$ curve will have a constant, non-zero slope. A plot with a parabolic shape or gradually changing slope illustrates that the orbital period is changing over time. A possible physical explanation for such behavior is the decay or expansion of the orbit of the binary system (see Chapter 4.8).

In addition, $O - C$ curves can exhibit sinusoidal variations that suggest periodic deviations to the orbital period of the binary. A possible explanation for such apparent or real changes in the binary period is the presence of a third star in the system. The Roemer delay, an effect due to the finite speed of light, may be the cause of apparent deviations to the orbital period (Roemer 1676). The presence of a third star can also cause Newtonian perturbations to the binary orbit, producing actual, physical changes to the binary period. Numerous analytic expressions have been developed for the case of a third body perturbing the orbit of a circular binary (Brown 1936; Harrington 1968, 1969; Soderhjelm 1975, 1982, 1984; Borkovits et al. 2003, 2011; Agol et al. 2005). An example $O - C$ curve for an eclipsing binary from the *Kepler* catalog which exhibits such periodic variations is shown in Figure 1-7. The binary, KIC 6525196, is part of the Rappaport et al. (2013) study of triple-star candidates among the sample *Kepler* binaries.

Another possible cause of apparent deviations to the orbital period is the migration of starspots on the surfaces of at least one of the component stars of short-period binaries, especially contact binaries (Kalimeris et al. 2002). It was shown by Kalimeris et al. that the perturbations to the $O - C$ curves would generally have amplitudes smaller than $\sim$0.01 days, and could appear to be quasi-periodic on timescales of an order of a few hundred days if the spot migration is related to differential rotation of the host star. In this thesis, we substantially expand on the earlier work of Kalimeris et al. regarding the measured and modeled properties of $O - C$ curves in contact binaries due to migratory starspots.

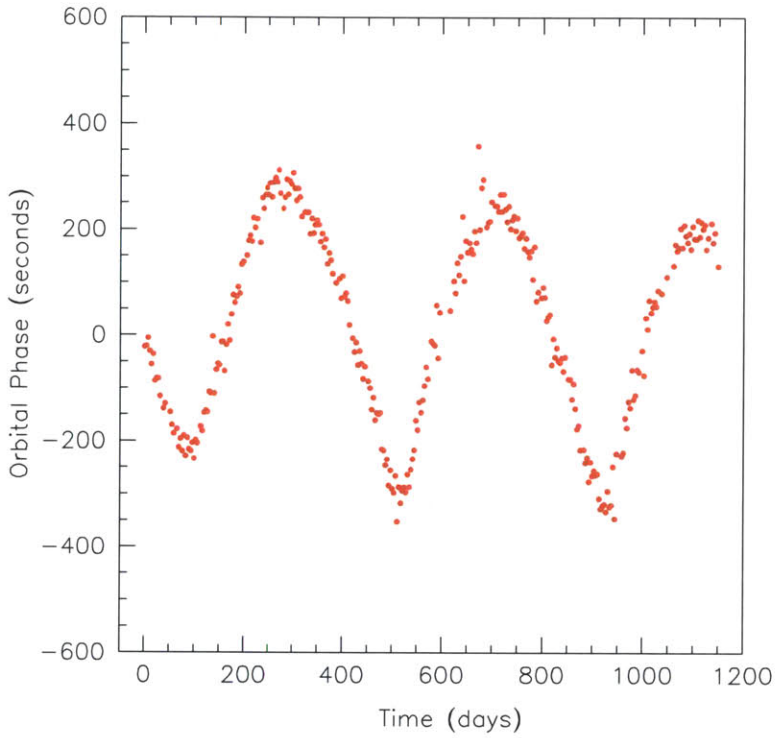

Figure 1-7: An $O - C$ curve for KIC 6525196, a *Kepler* eclipsing binary, that exhibits periodic variations which indicate evidence for the presence of a third star, as discussed in Rappaport et al. (2013).

1.3 The *Kepler* Mission

Since its launch in 2009, the NASA *Kepler* mission has been monitoring the visible-light flux of more than 150,000 stars (Borucki et al. 2010; Koch et al. 2010; Caldwell et al. 2010). The mission has carried out nearly continuous observations, with exquisite photometric precision of 1 part in 10^4, producing a data set that is unprecedented in the history of astronomy.

The *Kepler* satellite, illustrated in Figure 1-8, is a high-precision Schmidt telescope design with a 0.95-meter aperture[1]. The spacecraft is in an Earth-trailing heliocentric orbit, which allows the satellite to carry out nearly continuous monitoring of a fixed field of view on the sky, approximately 100 square degrees in size, as shown in Figure 1-9 [2]. The focal plane detector, which images this field, consists of 42 CCDs, each 50 by 24 millimeters in size, which are read out every six seconds. The data from these read-outs are integrated for thirty minutes and stored on board, to be transmitted to Earth once per month. As of now, fifteen quarters of data from the mission have been released to the public.

The main objective of the *Kepler* mission is to discover Earth-like exoplanets. To accomplish this, the satellite monitors the intensity of many stars while searching for periodic dimming on the order of 1% or less, caused when an exoplanet crosses our line of sight in front of the star. By analyzing such planet transits, the *Kepler* team has discovered over 2600 new exoplanets (Batalha et al. 2013). Many of these are in multi-planet systems.

The same method can be used to detect eclipsing binary systems, whose light curves also exhibit periodic dimming when one star passes in front of the other along our line of sight. Therefore, in addition to producing valuable data in the search for exoplanets, the *Kepler* mission has been monitoring nearly 3000 eclipsing binaries that happen to lie in the *Kepler* field (Slawson et al. 2011; Matijevič et al. 2012). Of this number of binary systems, about 470 have been classified as contact binaries

[1] `http://kepler.nasa.gov/Mission/QuickGuide/MissionDesign/PhotometerAndSpacecraft/`

[2] `http://kepler.nasa.gov/Science/about/targetFieldOfView/`

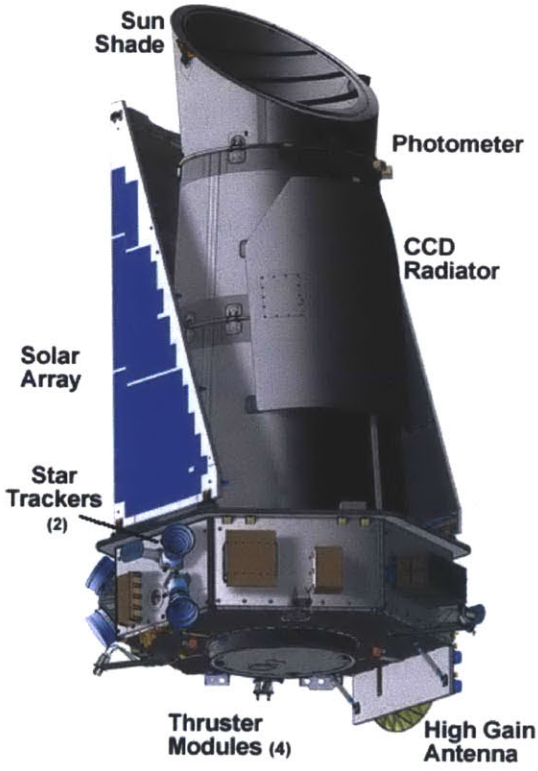

Figure 1-8: An artist's rendition of the *K*epler spacecraft.

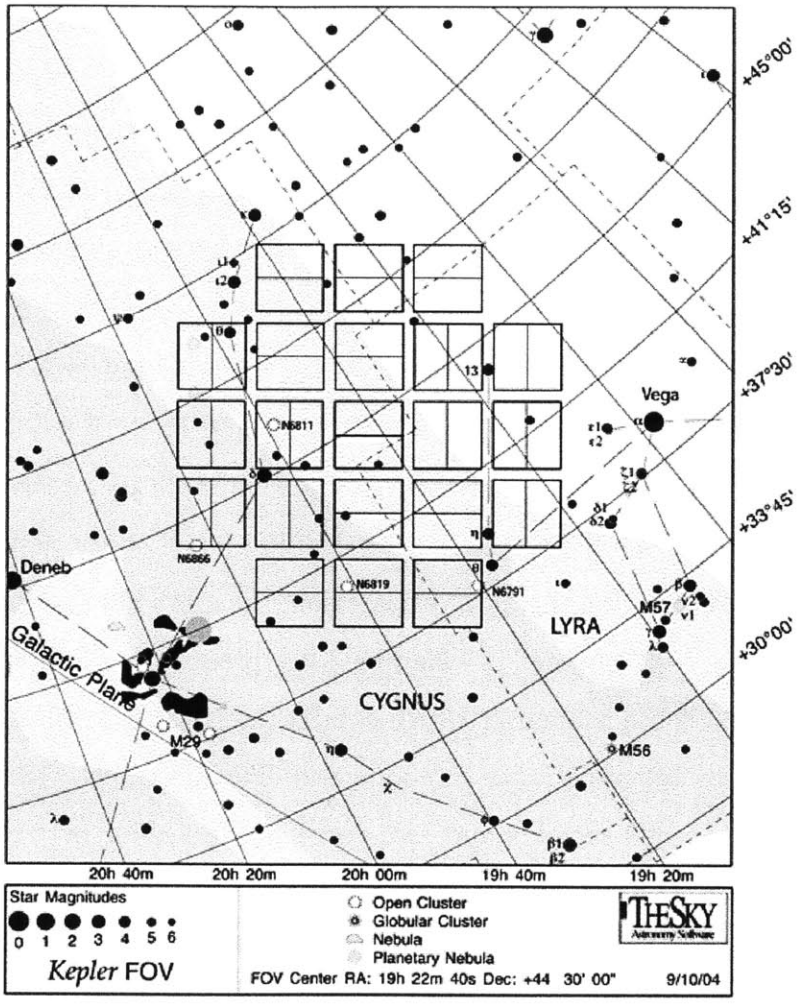

Figure 1-9: A map of the location of the *K*epler field of view on the sky. The rectangles indicate the arrangement of the satellite's 42 CCDs.

(Slawson et al. 2011). These are the principal focus of this thesis.

The original lifetime for the *Kepler* mission was four years. However, NASA announced the successful completion of *Kepler*'s prime mission and has begun carrying out an extended mission, possibly extending the lifetime of the project for another four years[3].

In this thesis, we report on a study of the timing of eclipses of contact binaries in the *Kepler* catalog. The major part of this work is adapted from "The Anticorrelated Nature of the O-C Curves for the Kepler Contact Binaries", by K. Tran, A. Levine, S. Rappaport, T. Borkovits, Sz. Csizmadia, and B. Kalomeni, which has just been submitted for publication to the Astrophysical Journal. This was a collaborative effort with Prof. Saul Rappaport and Dr. Alan Levine of M.I.T, Prof. Tamas Borkovits of the Baja Astronomical Observatory (Hungary), Dr. Szilard Csizmadia of the Institute of Planetary Research (German Aerospace Center), and Prof. Belinda Kalomeni of the University of Ege (Turkey). I carried out the vast majority of the data analysis and the preparation of the figures, as well as drafting much of the paper.

In Chapter 2, we describe the data preparation, the method of eclipse timing, and the production of $O-C$ curves. In Chapter 3, we present an illustrative sample of $O-C$ curves for 32 contact binaries which exhibit interesting features. These curves are characterized by quasi-periodic, random walk-like variations with typical semi-amplitudes of 200 to 300 seconds and anti-correlated behavior between the $O-C$ curves of the primary and secondary eclipse minima. In Chapter 4, we consider several explanations for the behavior of the $O-C$ curves and extend the work of Kalimeris et al. (2002) using a simple geometric model of a starspot on one of the stars.

[3]http://www.nasa.gov/home/hqnews/2012/nov/HQ_12-394_Kepler_Completes_Prime_Mission.html

Chapter 2

Data Analysis

This chapter will provide a description of the light curve data obtained from the *Kepler* archive and the methods of noise reduction which were used to prepare the data for analysis. It will explain the algorithm used to calculate the timing of eclipses. As a result, over 2000 $O-C$ curves were generated for the primary and secondary eclipses of all the objects in the latest *Kepler* eclipsing binary catalog, of which a smaller sample of contact binaries were selected for further analysis. The next chapter will discuss in more detail the manner in which this sample of objects was selected and the key features of their $O-C$ curves.

2.1 *Kepler* Data

This thesis is based on *Kepler* long-cadence light curves, which are time series data of flux measurements of target objects. *Kepler* data are comprised of either short-cadence (SC) or long-cadence (LC) light curves, which are summed for 1 minute and 30 minutes respectively. We used data from Quarter 1 through Quarter 13, which spans more than three years of the *Kepler* mission. The start dates[1] for each quarter is listed in Table 2.1. *Kepler* objects are typically referred to by a seven or eight-digit *Kepler* Input Catalog (KIC) number.

[1] `http://archive.stsci.edu/mast_faq.php?mission=KEPLER`

Quarter Number	Actual Start Date
1	May 13, 2009
2	June 18, 2009
3	September 18, 2009
4	December 19, 2009
5	March 19, 2010
6	June 23, 2010
7	September 23, 2010
8	December 22, 2010
9	March 24, 2011
10	June 27, 2011
11	September 29, 2011
12	January 5, 2012
13	March 29, 2012
14	June 28, 2012
15	October 4, 2012

Table 2.1: The actual start dates (UTC) for each *Kepler* quarter, up to Quarter 15. The end dates are typically one day before the start of the next quarter. The data used in this thesis spans Quarter 1 through Quarter 13.

2.1.1 Data Preparation

We obtained long-cadence light curve data for all the candidates in the latest *Kepler* eclipsing binary catalog (Slawson et al. 2011) that were available at the Multimission Archive at STSci (MAST)[2]. These lightcurves were made with the PDC-MAP algorithm (Stumpe et al. 2012; Smith et al. 2012), which is intended to remove instrumental signatures from the flux time series while retaining the bulk of the astrophysical variations of each target.

To be able to use all of the data from each quarter coherently, it was necessary to create a single data file for analysis. For each quarter, the flux time series was normalized to its median value. Then, the data for each quarter was concatenated together to create one file spanning all of the quarters.

We also applied a high-pass filter to the flux time series in order to remove intensity components with frequencies below half of the binary frequency while leaving periodically recurring features of the light curve unaffected. A smoothed light curve

[2]`http://archive.stsci.edu/kepler/data_search/search.php`

was generated by taking running average, or, that is, by convolving the data with boxcar function of duration equal to the known binary period. Then, the smoothed light curve was subtracted from the unsmoothed data.

2.2 Eclipse Timing

Because long-cadence data provides relatively coarse time resolution, we calculated eclipse times with an interpolation method consisting of a parabolic fit to local minima in the flux time series. The time of the minimum of the fitted parabola was used to time the eclipse. This algorithm provides excellent accuracy for short-duration eclipses, but loses some accuracy when the eclipse duration is longer than 10 long-cadence samples. For the contact binaries we analyze in this thesis, which have orbital periods that range between 0.2 to 0.4 days, the algorithm works well and typically yields eclipse times subject to a root mean square scatter of $\sim$30 seconds.

This interpolation algorithm of eclipse timing begins with calculating a phase range to determine whether local minima in the flux time series correspond to the primary eclipse of the binary. To accomplish this, the data were folded based on the known period obtained from the Slawson et al. (2011) *Kepler* eclipsing binary catalog. The primary eclipse was identified by finding the lowest flux points of the folded light curve and the phase of the primary eclipse was determined by fitting a parabola to those points and using the minimum of the fit. A phase range was selected based on this calculated phase of the primary eclipse. In addition, a flux threshold was determined using the value of the depth of the primary eclipse in the folded light curve.

We then searched the unfolded time series data to find eclipses, selecting out local minima which had flux values below our determined threshold. More accurate times of these local minima were determined by fitting a parabola to the lowest three flux points and using the minimum of the fit. The previously determined phase range was used to select which of these minima corresponded to the primary eclipse.

In addition, $O - C$ curves would also be generated for the secondary eclipse and

the maxima of the light curve. To time the secondary eclipse and maxima, we used an analogous process, shifting the phase range used to search the flux time series data by an appropriate phase—180° for the secondary eclipse and 90° or 270° for each maxima.

2.3 Generating $O - C$ Curves

The $O - C$ curve was formed by taking the determined observed eclipse times for each object and the previously published orbital period from the *Kepler* eclipsing binary catalog (Slawson et al. 2011). We subtracted from the eclipse times a linear function consisting of the eclipse cycle count times the constant orbital period, that is, a calculated expected time of eclipse based on the known period. A linear function was then fit to this preliminary $O - C$ curve to obtain the best value for the average orbital period over the duration of the data series. From the fit, we determined a corrected value for the known period and generated a final $O - C$ curve using this corrected period.

In addition to the $O - C$ curves for the primary eclipse, $O - C$ curves were also produced for the secondary eclipse and the maxima of the light curve. These curves were generated with a completely analogous process. However, it is important to note that to make the curves for the secondary eclipse and the maxima, we utilized the corrected value for the previously published orbital period determined from making the $O - C$ curve for the *primary* eclipse.

We applied a low-pass filter to the final $O - C$ curves. A smoothed light curve was generated by convolving the data with a boxcar function of a five-day duration. The smoothing process reduced high-frequency variations in the $O - C$ curves, while most of the interesting features of the curves occur on timescales of weeks to months.

Chapter 3

$O - C$ Curves for Contact Binaries

The eclipse timing analysis on the set of *Kepler* eclipsing binaries produced a large variety of curves with numerous interesting features. In particular, the $O - C$ curves for contact binaries were discovered to exhibit several characteristics which make them easily distinguishable from the $O - C$ curves of other binaries. The notable properties of these curves include quasi-periodic or random-walk like variations with typical amplitudes of $\pm$ 200 to 300 seconds. In addition, we find that the $O-C$ curves for the primary and secondary eclipses often show highly anti-correlated behavior.

3.1 Selected Illustrative Sample

We selected a collection of $O - C$ curves that were most illustrative of the features characteristic to contact binaries. This sample of 32 curves was selected for having quasi-periodic or random-walk like variations and orbital periods in the range of 0.25 to 0.45 days. It was found that systems which exhibited quasi-periodic or random-walk like behavior would typically satisfy our condition on the orbital period. The selected sample were also found to exhibit apparent anti-correlated behavior between the $O - C$ curves of the primary eclipse and the secondary eclipse. A second, later search through all the $O - C$ curves for the entire set of eclipsing binaries, now selecting for anti-correlated behavior between the primary and secondary eclipses, would result in identifying systems that fulfill our first set of selection criteria.

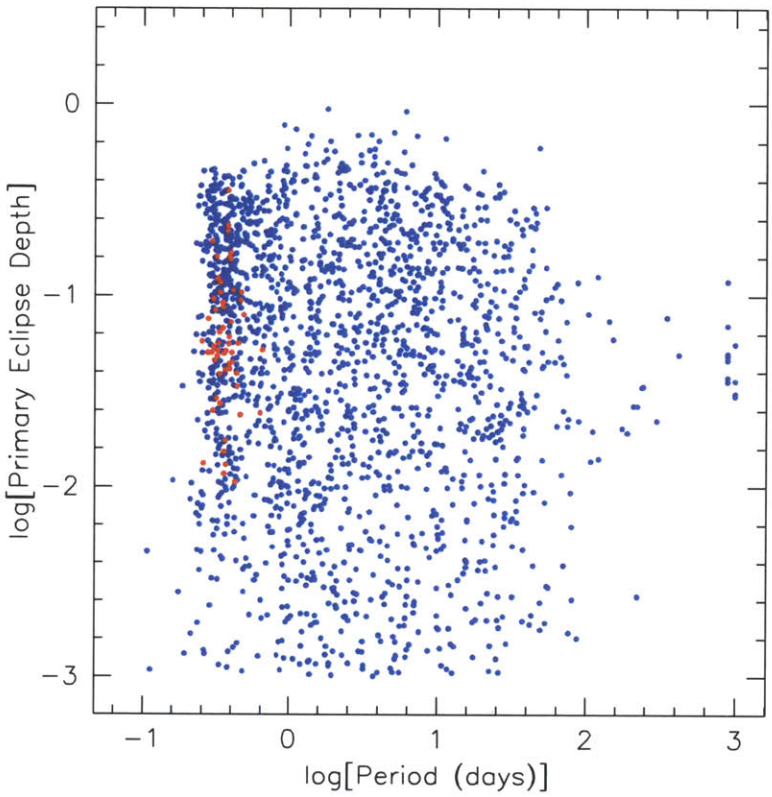

Figure 3-1: The primary eclipse depth of the Slawson et al. (2012) binary stars plotted against their orbital period, shown in blue. Our selected sample of binaries are marked in red.

A summary of our selected sample of *Kepler* eclipsing binaries can be found in Table 3.1. Of these 32 systems, 21 are classified as overcontact (OC) binaries, 8 as ellipsoidal (ELV) binaries, and 3 as an uncertain type of binary. Figure 3-1 plots the binary orbital period against the primary eclipse depth for the catalog of eclipsing binary systems and illustrates how our selected sample compares to the entire set. The set of $O - C$ curves of these 32 objects, which exhibit all the characteristic features for contact binaries, is shown in Figures 3-2–3-5.

3.2 Quasi-periodic, random walk-like variations

The $O - C$ curves of our selected sample exhibit distinct quasi-periodic and random-walk like variations. The characteristic timescale of these quasi-periodic variations

KIC Number	Orbital Period (days)	Type	Kepler Magnitude	Temperature (K)	Correlation Coefficient
1873918	0.3324	OC	13.715	5715	0.42
2017803	0.3057	OC	14.614	5056	-0.50
2159783	0.3738	OC	14.965	5643	-0.16
2715007	0.2971	OC	14.730	5598	0.10
3837677	0.4619	OC	15.548	5466	-0.46
3853259	0.2766	OC	13.922	4467	-0.42
4937350	0.2937	OC	14.273	5862	-0.60
5008287	0.2919	ELV	15.313	5881	-0.34
5022573	0.4417	OC	11.474	5648	-0.13
5033682	0.3799	UN	13.258	5611	-0.63
5283839	0.3152	OC	15.156	5906	0.09
6964796	0.3999	OC	12.611	5657	-0.52
7118656	0.3213	OC	15.033	5271	-0.24
7217866	0.4072	OC	13.865	5600	-0.15
7542091	0.3904	OC	12.343	5673	-0.31
7691553	0.3483	ELV	14.620	5786	-0.48
7773380	0.3076	ELV	14.475	5357	-0.40
8190613	0.3326	OC	15.126	5384	-0.28
8956957	0.3244	ELV	13.978	6307	-0.72
9020289	0.3840	OC	14.741	5997	-0.60
9071104	0.3852	OC	13.651	5959	-0.52
9097798	0.3341	OC	14.581	5592	-0.41
9451598	0.3623	OC	13.627	6060	-0.77
9519590	0.3309	OC	13.916	5961	-0.24
9821923	0.3495	ELV	14.210	5730	-0.53
9832227	0.4580	UN	12.260	5854	-0.19
10148799	0.3466	ELV	15.409	5340	-0.66
10155563	0.3603	ELV	11.992	5982	- 0.03
11013608	0.3183	OC	12.566	6223	-0.33
12055421	0.3856	ELV	12.519	6118	-0.47
12418274	0.3527	OC	14.349	5215	0.22
12598713	0.2572	UN	12.762	5189	-0.14

Table 3.1: A table of the objects in our selected sample of $O - C$ curves, listing the following information: KIC number; orbital period; type—detached (D), semi-detached (SD), overcontact or contact (OC), ellipsoidal (ELV), and uncertain (UN); *Kepler* magnitude; effective temperature; and correlation coefficient of the $O - C$ curves of the primary and secondary eclipses.

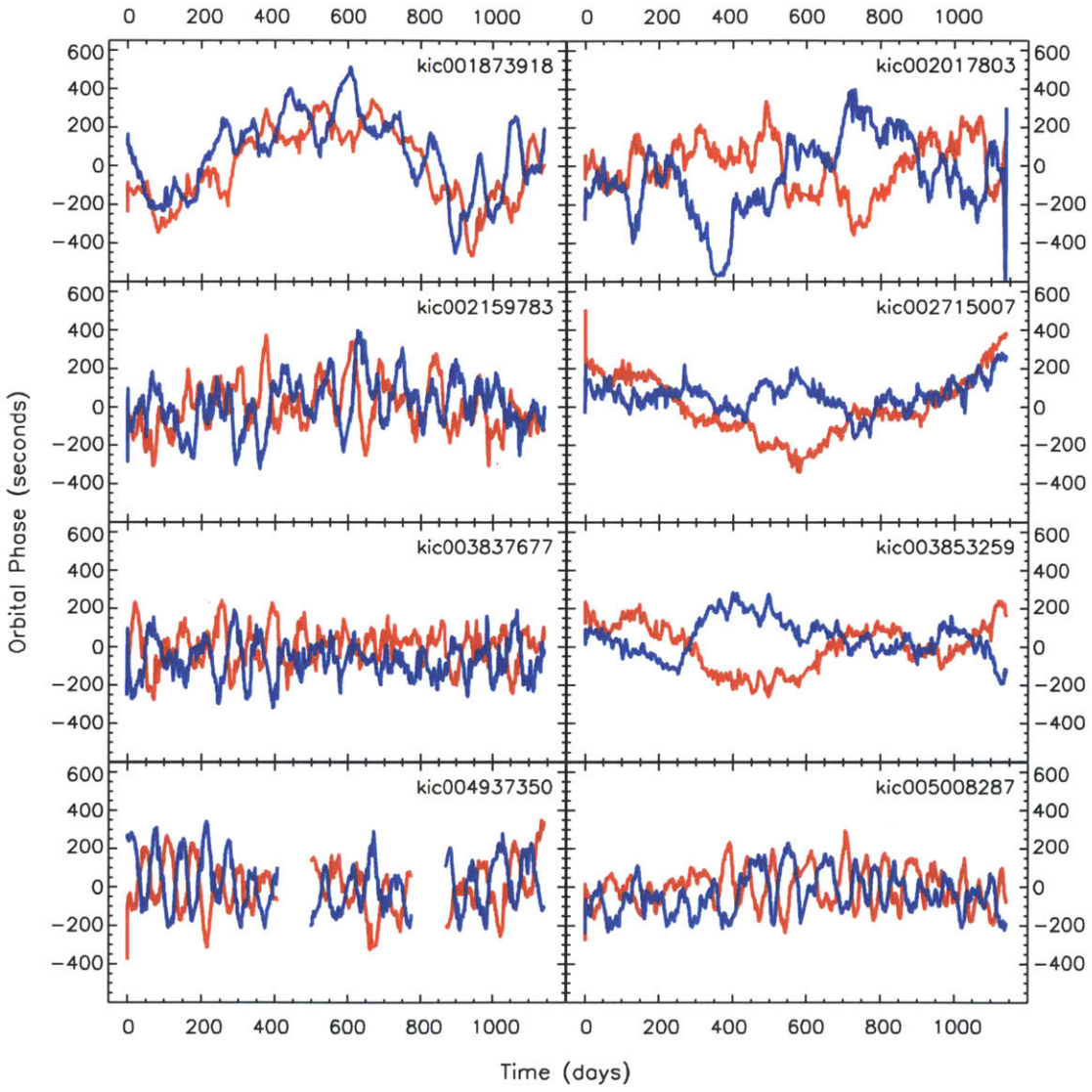

Figure 3-2: The $O - C$ curves for a sample of eight *Kepler* binary systems with KIC numbers in the range of 1873918 to 5008287. The $O - C$ curves for the primary and secondary eclipses are plotted as red and blue curves, respectively. Like typical $O-C$ curves for contact binary systems, these curves exhibit random-walk like, quasi-periodic behavior. In addition, the curves for the primary and secondary eclipses are anti-correlated on shorter timescales.

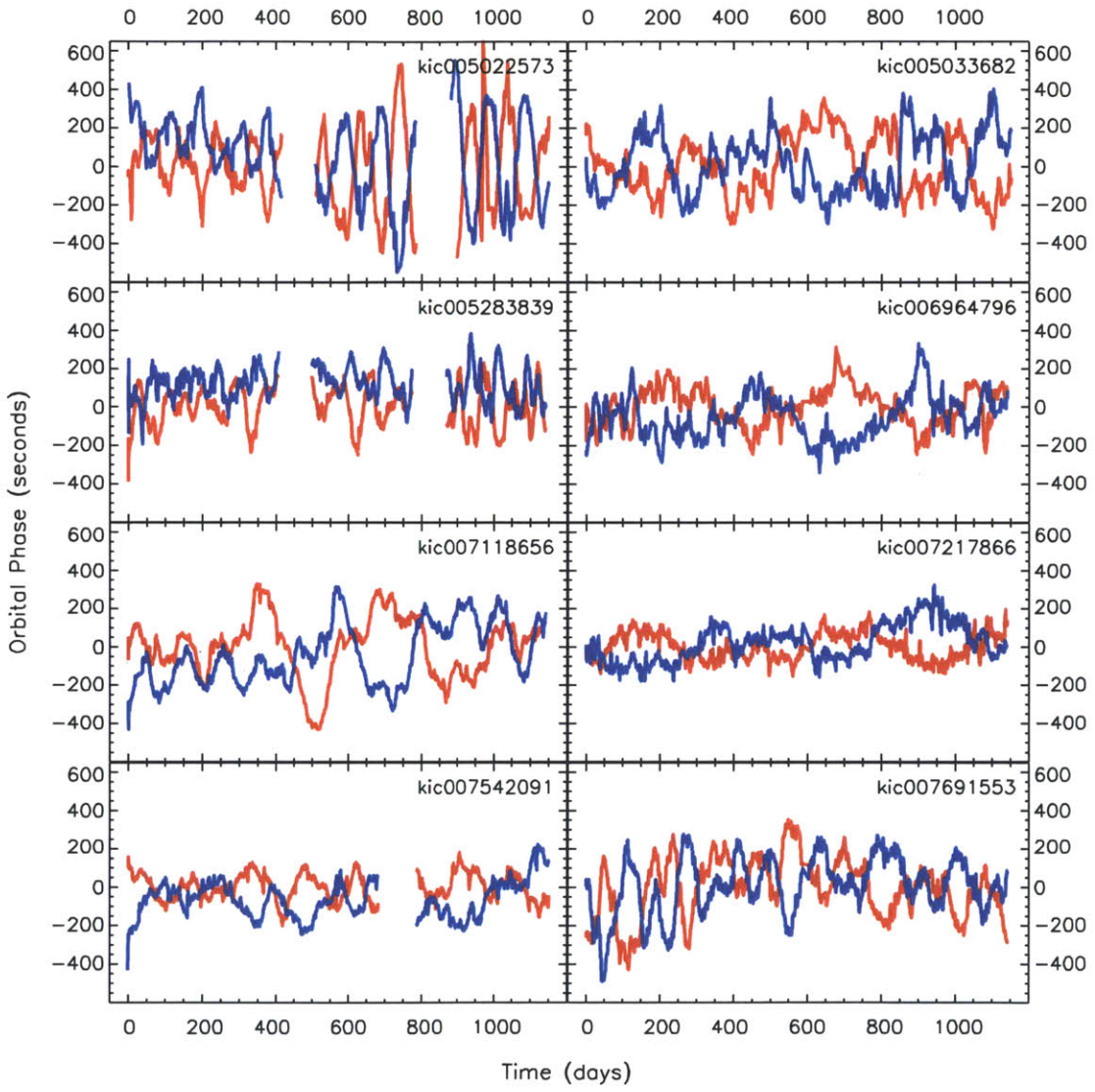

Figure 3-3: The $O - C$ curves for a sample of eight *Kepler* binary systems with KIC numbers in the range of 5022573 to 7691553. The $O - C$ curves for the primary and secondary eclipses are plotted as red and blue curves, respectively. Like typical $O-C$ curves for contact binary systems, these curves exhibit random-walk like, quasi-periodic behavior. In addition, the curves for the primary and secondary eclipses are anti-correlated on shorter timescales.

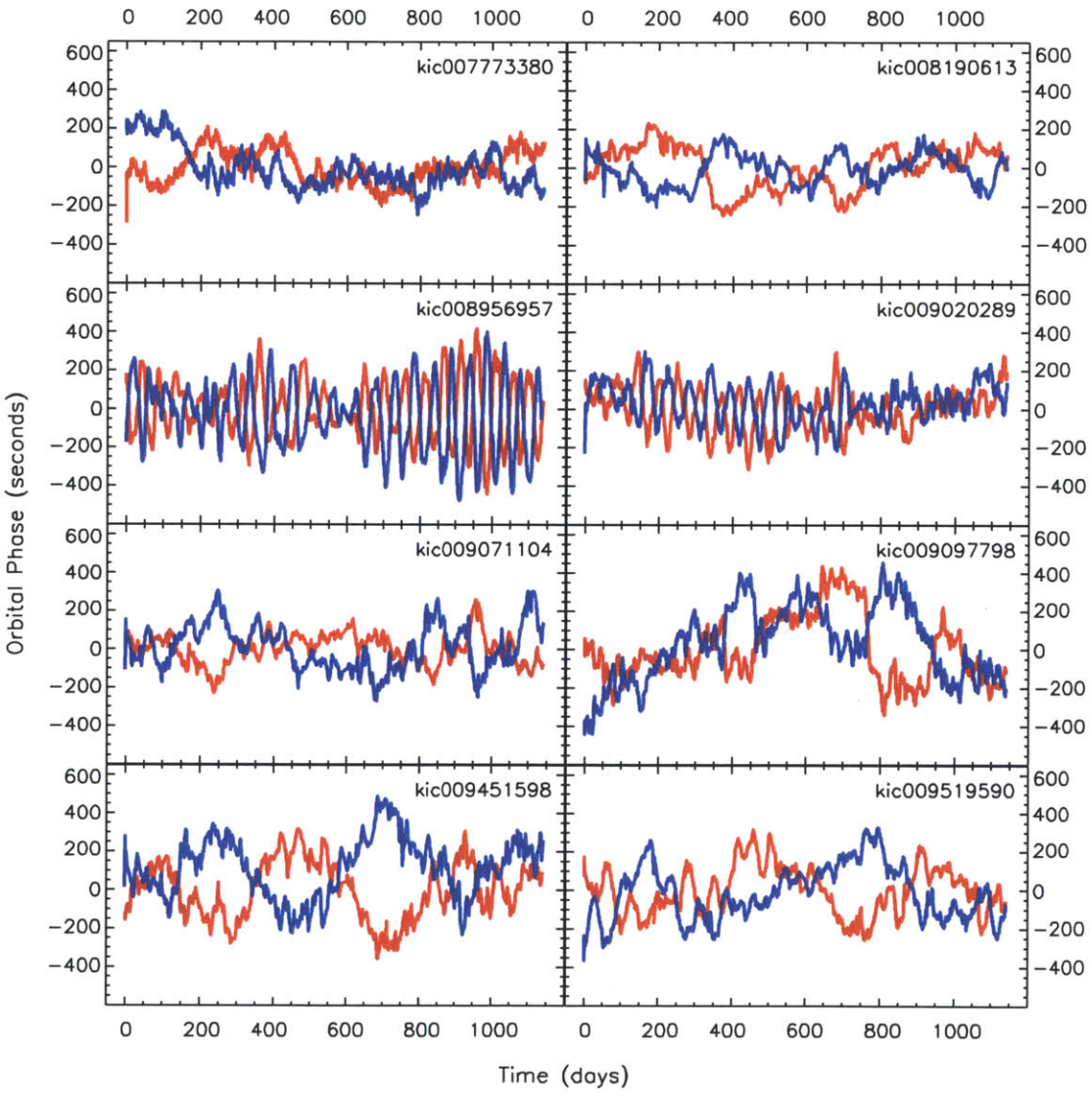

Figure 3-4: The $O - C$ curves for a sample of eight *Kepler* binary systems with KIC numbers in the range of 7773380 to 9519590. The $O - C$ curves for the primary and secondary eclipses are plotted as red and blue curves, respectively. Like typical $O-C$ curves for contact binary systems, these curves exhibit random-walk like, quasi-periodic behavior. In addition, the curves for the primary and secondary eclipses are anti-correlated on shorter timescales.

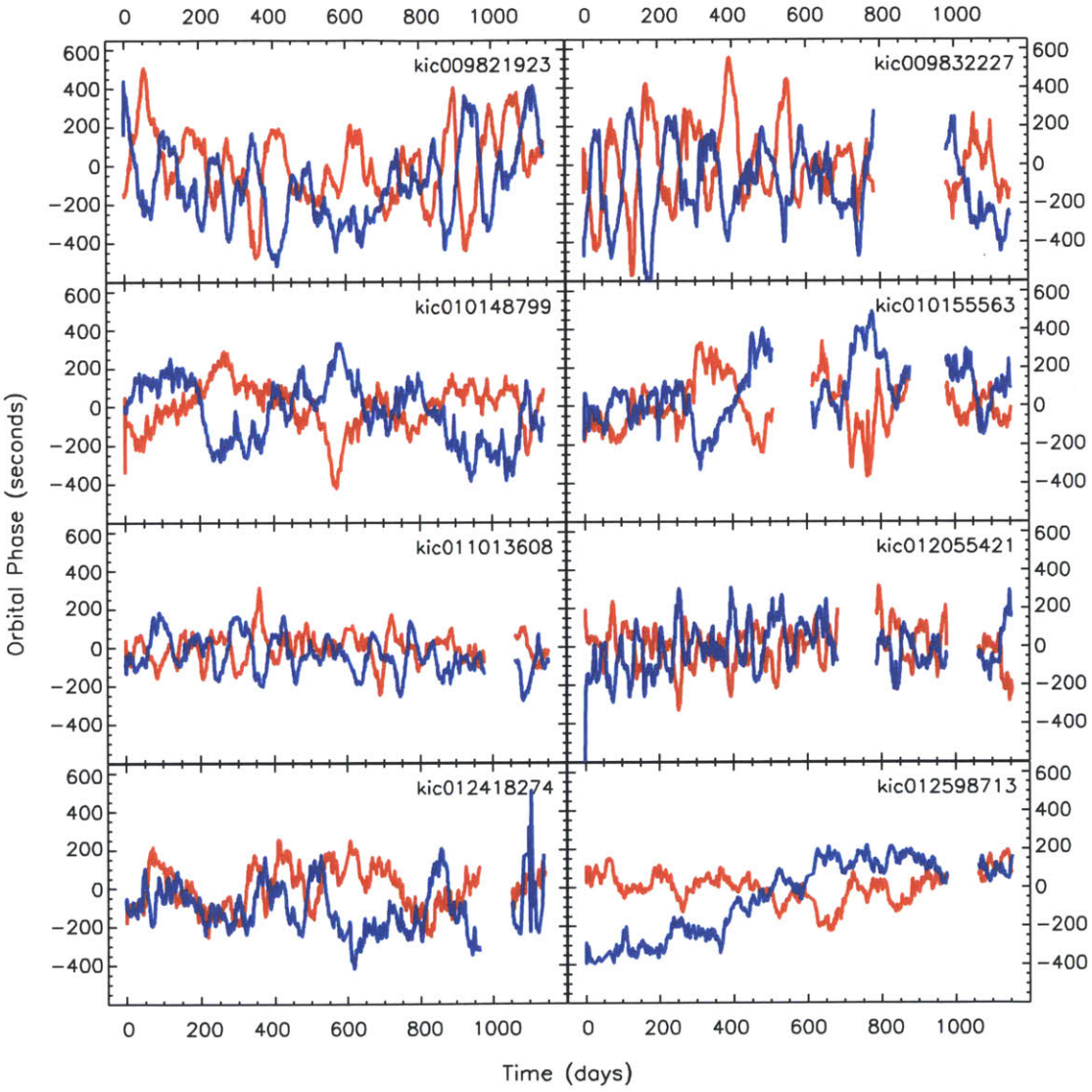

Figure 3-5: The $O - C$ curves for a sample of eight *Kepler* binary systems with KIC numbers in the range of 9821923 to 12598713. The $O - C$ curves for the primary and secondary eclipses are plotted as red and blue curves, respectively. Like typical $O-C$ curves for contact binary systems, these curves exhibit random-walk like, quasi-periodic behavior. In addition, the curves for the primary and secondary eclipses are anti-correlated on shorter timescales.

can vary greatly, but many curves have quasi-periods in the range of 20 to 200 days.

For a more thorough analysis of these quasi-periodicities, we carried out a Fourier transform of each $O-C$ curve. The transformation was performed in order to analyze the high-frequency variations that the smoothing process would otherwise reduce. We found no strong peaks in the Fourier spectrum, except at frequencies associated with known beats between the orbital period and the *Kepler* long-cadence sampling time. When plotting the Fourier amplitude against the frequency on a log-log scale, we find that the amplitudes have a log-log slopes of ~-1.0 to -1.3, similar to Fourier spectra associated with random-walk like behavior. The Fourier transforms for the $O-C$ curves of one example system, KIC 5033682, can be seen in Figure 3-6.

These variations also typically have semi-amplitudes of about 200 to 300 seconds. However, a few systems have somewhat higher amplitude variations, such as KIC 5022573, which can be seen in the top panel of Figure 3-3, and KIC 9832227, which can be seen in the top panel of Figure 3-5. Some $O-C$ curves have larger amplitudes due to longer timescale trends over the duration of the data sample, such as KIC 1873918, which can be seen in the top panel of Figure 3-2, and KIC 9097798, which can be seen in a middle panel of Figure 3-4. However, when we look at the behavior of these curves over shorter timescales, the semi-amplitudes of the variations still fall within typical range of about 200 to 300 seconds.

3.3 Anti-correlated Behavior

The $O-C$ curves of our selected sample also exhibit highly anti-correlated behavior between the curves for the primary and secondary eclipses. This anti-correlation occurs on shorter time scales and over at least some portion of the data set. As discussed earlier, some curves have longer timescale trends, typically over 800 days or greater. While all the curves exhibit some anti-correlated behavior on shorter timescales, the sets of curves can become positively correlated in these longer timescale variations. Examples of sets of $O-C$ curves which are positively correlated on longer timescales are KIC 1873918, which can be seen in the top panel of Figure 3-2, and

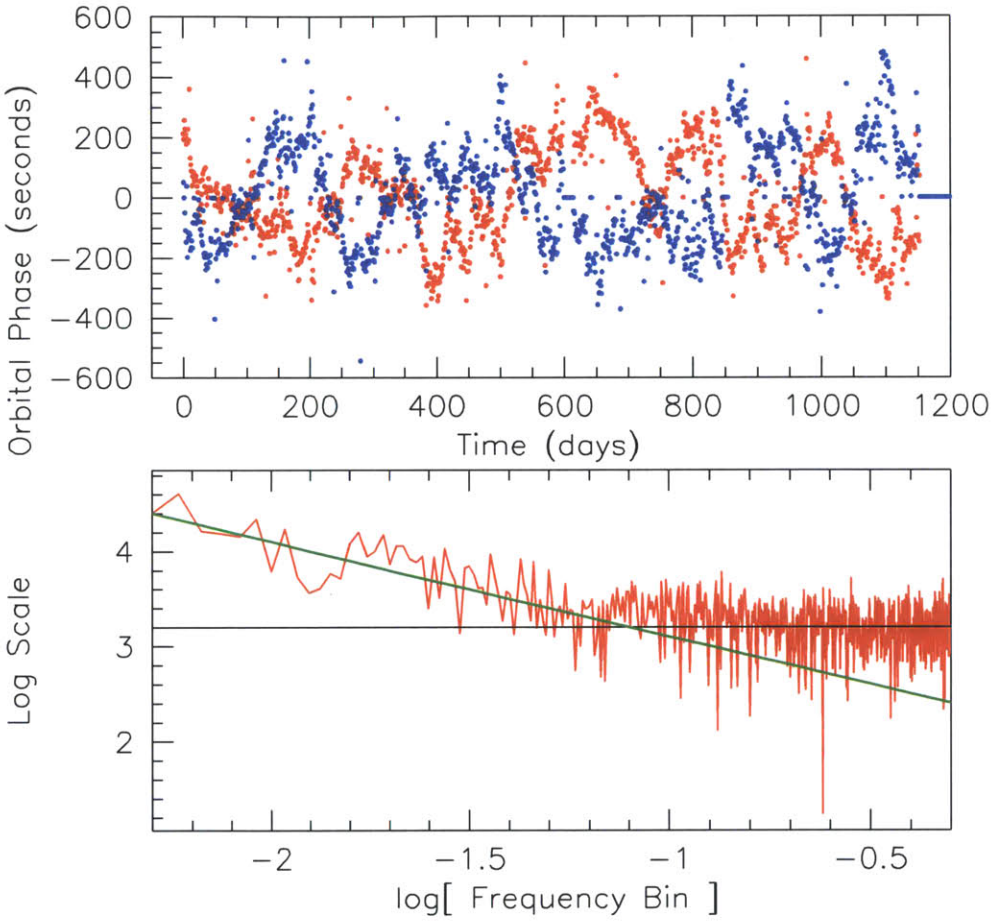

Figure 3-6: The $O-C$ data for the primary and secondary eclipses of KIC 5033682 (top panel) as well as their Fourier transform for the primary eclipse curve plotted on a log-log scale (bottom panel). Being interested in the $O-C$ variations on the shorter timescale of 20 to 200 days, we plotted the frequency range of 0.05 to 0.5. The log-log slopes of the plots were measured to be ~ -1.0 to -1.3, similar to Fourier spectra associated with random-walk like behavior. The black horizontal line in this figure represents the constant background and the green line shows the -1.0 slope.

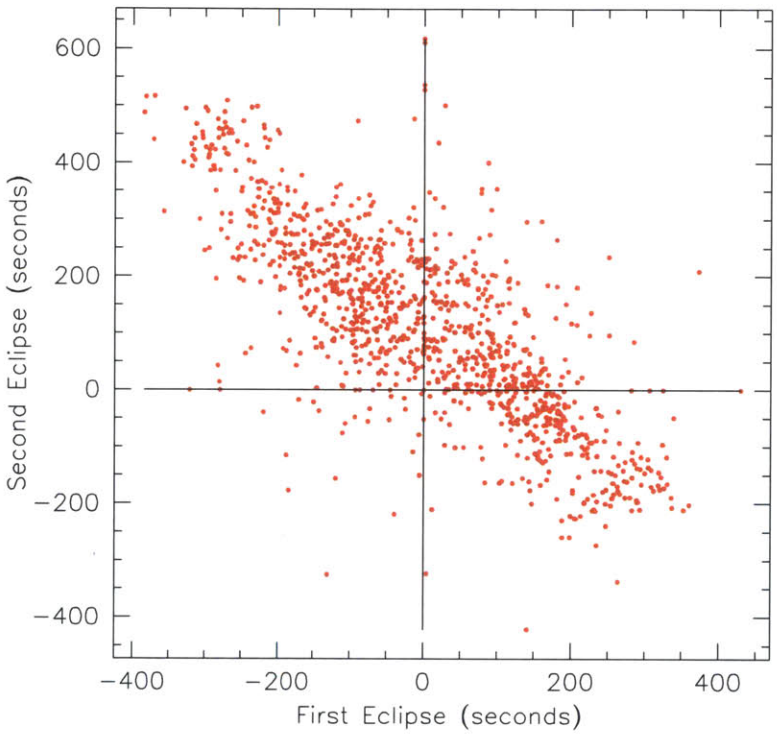

Figure 3-7: A point-by-point correlation plot of the binned $O - C$ curves for the primary and secondary eclipses of KIC 9451598. The negative slope of the plot, -0.77, clearly demonstrates the anti-correlation of the $O - C$ curves.

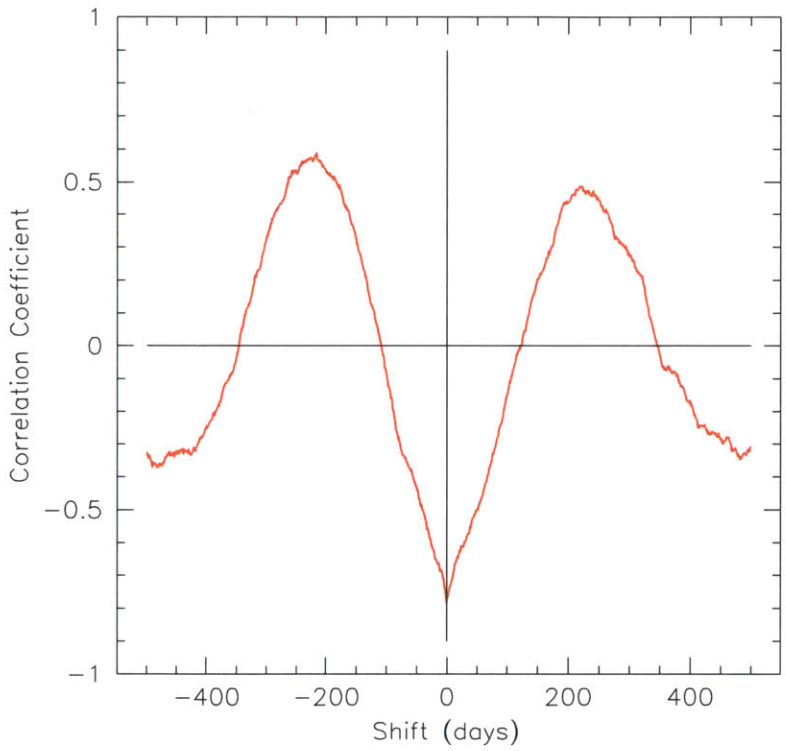

Figure 3-8: A formal cross correlation function for the $O - C$ curves for the primary and secondary eclipses of KIC 9451498. The function has a minimum at the zero time shift, quantitatively showing that the set of curves has a strong negative correlation. The value of this minimum, which is the correlation coefficient of the curves with no time shift, is -0.77.

KIC 9821923, which can be seen in the top panel of Figure 3-4.

We carried out a more quantitative analysis of this anti-correlated behavior by calculating formal correlation coefficients and cross correlation functions for the sets of curves in our selected sample. To calculate these coefficients and functions, the data points of the $O-C$ curves were first placed in one-day bins. The calculated coefficients are shown in Table 3.1. Not all systems have a negative correlation coefficient, due to overall correlated behavior on longer timescales. For systems that are dominated by anti-correlated behavior, the correlation coefficients range from -0.03 to -0.77. A point-by-point correlation plot for an example system, KIC 9451598, can been seen in Figure 3-7. The plot shows a clear anti-correlation between the data of the $O-C$ curves of the primary and secondary eclipses. A cross correlation function for this object can be seen in Figure 3-8, which demonstrates more quantitatively the negative correlation between the set of $O-C$ curves. The function plots the correlation coefficient of the two curves as a function of a time shift applied to one of the curves.

For our selected sample of binaries, $O-C$ curves were also calculated for the two maxima of the light curve in each orbital cycle. As discussed in the Introduction, the characteristic shape of the light curves of contact binaries is nearly sinusoidal. Because there are no well-defined out-of-eclipse regions to the light curve, it is possible not only to identify distinct minima in the curves, but also maxima.

The $O-C$ curves were generated for the maxima using the same eclipse timing algorithm as discussed in the previous chapter. The set of $O-C$ curves for the two maxima as well as the two eclipse minima for one example object, KIC 9451598, is shown in Figure 3-9. The $O-C$ curves for the eclipse maxima are clearly anti-correlated with respect to each other in the same way that the set of curves for the minima are also anti-correlated. In addition, the plot shows that the $O-C$ curves of the maxima are offset in phase from the curves of the minima by about 90°. A possible explanation for these phase shifts and the observed anti-correlated behavior will be discussed in the following chapter.

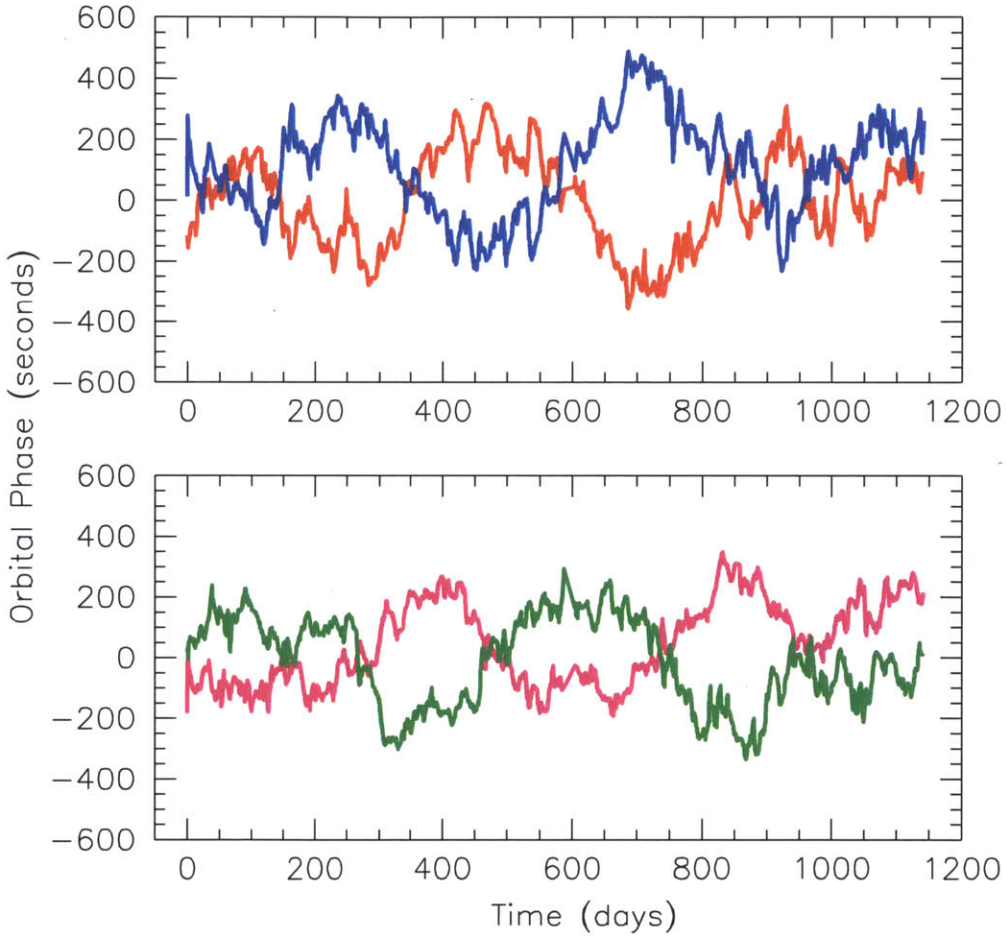

Figure 3-9: The $O - C$ curves for the minima (top panel) as well as the maxima (bottom panel) of KIC 9451598. The set of curves for the maxima exhibit anti-correlated behavior with respect to each other in the same way that the set of curves for the minima also exhibit anti-correlated behavior. In addition, the curves for the minima are $\sim 90°$ out of phase with respect to the curves for the maxima.

Chapter 4

Models

4.1 Period Changes

The behavior exhibited in the $O-C$ curves for the contact binaries cannot represent actual changes in the orbital periods (Kalimeris et al. 2002). For circular orbits like those expected for contact binaries, period changes would produce similar effects in both the primary and secondary $O-C$ curves, which therefore should be positively correlated. Therefore, the variations associated with this anti-correlated behavior cannot be the result of orbital period changes.

We can consider if mass transfer could drive such rapid changes in the $O-C$ curves, even if the primary and secondary eclipses were not anti-correlated. If we represent a small portion of the $O-C$ curve as:

$$O - C \simeq \tau \sin(2\pi t/T) \tag{4.1}$$

where τ and T are rough measures of the amplitude and period of the $O-C$ variations, and t is the time. If the variations were caused by orbital period changes, the second derivative of the $O-C$ curve would be related to the first derivative of the orbital period as

$$\frac{\dot{P}_{\rm orb}}{P_{\rm orb}} = \frac{d^2}{dt^2}(O-C) = -\frac{4\pi^2}{T^2}\tau \sin(2\pi t/T). \tag{4.2}$$

It is straightforward to show that mass transfer in a binary results in $\dot{P}_{\rm orb}/P_{\rm orb} \approx \dot{M}/M$. Therefore, the implied mass transfer rate would be of order

$$\frac{\dot{M}}{M} \approx \frac{d^2}{dt^2}(O-C) \approx 4\pi^2 \frac{\tau}{T^2}. \tag{4.3}$$

For characteristic $O-C$ amplitudes of $\sim \pm 200$ seconds and cycle times of $\sim$50 to 200 days, we find implied mass transfer rates of $\dot{M}/M \simeq 0.001 to 0.01$ yr^{-1}. Such rates are implausibly large even for a contact binary.

4.2 Slightly Eccentric Orbits

The orbits of contact binaries must generally be circular or nearly circular, but it is possible that a physical process, such as perturbations from a third body in the system or a magnetic event, could induce a slight eccentricity in the orbit from time to time. The resulting apsidal motion would result in $O-C$ variations, to first order in eccentricity, with amplitudes of $\tau = \pm(P_{\rm orb}/2\pi)2e\cos\omega$ for the primary and secondary eclipse, respectively, where ω is the longitude of periastron (Gimenez & Garcia-Pelayo 1983). For an illustrative system of our sample, with an orbital period of 0.3 days and $O-C$ variations of amplitude $\pm$300 seconds, such variations require a minimum eccentricity of $\sim$0.04. Since this is implausibly high for a contact binary, slightly eccentric orbits are unlikely to be the cause of the apparent anti-correlated behavior exhibited by our selection of $O-C$ curves.

4.3 A Simple Starspot Model

4.3.1 Spot Visibility

We now consider a simple geometric model where a single starspot on one of the component stars of a binary might produce the anti-correlated behavior seen in the $O-C$ curves of the primary and secondary eclipses. The stars are assumed to be spherical and rotating synchronously with the orbit. The $\hat{z}$ direction is defined to be

parallel to the orbital angular momentum vector and the stars revolve in the $x-y$ plane. The observer is located in the $y-z$ plane and views the system with orbital inclination angle i. The unit vector in the direction from the system toward the observer is then $\vec{V} = \cos i\,\hat{z} + \sin i\,\hat{y}$. For a spot located at colatitude α, the angle from the stellar pole, and stellar longitude, ℓ, the unit vector pointing from the center of the star through the spot is $\vec{S} = \sin\alpha\,\sin(\omega t + \ell)\,\hat{x} + \sin\alpha\cos(\omega t + \ell)\,\hat{y} + \cos\alpha\,\hat{z}$, where ω is the orbital angular velocity. A starspot located at $\ell = 0°$ and $\alpha = 90°$ is defined to lie along the line segment connecting the two stellar centers.

We assume that the spot occupies a small portion of the surface of the star where it is located and that radiates in a Lambertian manner. The projected area of the spot normal to the line of sight is proportional to $\vec{V}\cdot\vec{S}$. If this dot product is negative, the spot is on the hemisphere of the star facing away from the observer and is therefore not visible. Neglecting the limb darkening, an effect where the observed brightness of a star diminishes towards its edges, the apparent brightness of the star is changed by the presence of the spot according to the expression

$$\Delta F = \epsilon\,[\cos\alpha\cos i + \sin\alpha\sin i\cos(\omega t + \ell)] \tag{4.4}$$

where ϵ is a constant with dimensions of flux, assumed to be much less than the overall flux from the binary. In order for the spot to remain continuously visible, ΔF must always be positive. This visibility condition requires that $\cos\alpha\cos i > \sin\alpha\sin i$, or $\alpha + i < 90°$.

4.3.2 Analytic Estimate of the $O-C$ Amplitudes

When no spots are present, the light curve of a contact binary may be represented with sufficient accuracy by

$$\mathcal{B} = -B\cos 2\omega t \tag{4.5}$$

where time $t = 0$ corresponds to the time of primary eclipse, which is indistinguishable from the secondary eclipse here, and the constant term has been dropped. In this model, B is the modulation amplitude due to both ellipsoidal light variations and eclipses.

When one spot is present, the observed flux as a function of time, neglecting constant terms, is

$$\mathcal{F} = -B\cos 2\omega t + \epsilon \sin\alpha \sin i \cos(\omega t + \ell). \tag{4.6}$$

It is straight forward to analyze how the two minima and maxima of the light curve are shifted in phase relative to the case of no spot, assuming that, as previously mentioned, $\epsilon \ll B$. We can find the four phase shifts, in radians, to be

$$\Delta\phi_{\min} = \pm\frac{\epsilon \sin\alpha \sin i}{4B} \sin\ell \tag{4.7}$$

$$\Delta\phi_{\max} = \mp\frac{\epsilon \sin\alpha \sin i}{4B} \cos\ell \tag{4.8}$$

for the first or second, respectively, minimum or maximum.

From these expressions, there is clear anti-correlation between the time shifts of the two minima as well as the two maxima, while the time shifts of the two maxima are 90° out of phase with respect to the times of the two minima. It is also clear from these expressions that the phase shifts depend on the spot longitude. A near uniform migration in longitude over time results in quasi-periodicities in the $O - C$ curve.

The amplitude of the observed $O - C$ variations as the spot migrates around the star at constant colatitude α can be computed from Equation (4.7) and is given in units of time by

$$\Delta\tau = \frac{\epsilon \sin\alpha \sin i}{4B}\frac{P_{\rm orb}}{2\pi} \tag{4.9}$$

The coefficient quantifying the photometric strength of the spot may be estimated by

$$\epsilon \simeq \frac{4\Delta T}{T}\frac{\pi r_{\rm spot}^2}{\pi R_1^2}\frac{B_0}{2} \tag{4.10}$$

where $r_{\rm spot}$ is the radius of the spot, R_1 is the radius of the star with the spot, ΔT is the decrement or increment in temperature of the starspot, and B_0 is the mean brightness of the binary. We define the eclipse depth in terms of the fractional decrease in intensity at eclipse minimum, $\xi \equiv B/B_0$, so that the expression for the amplitude of the $O-C$ variations becomes

$$\Delta\tau = \frac{1}{4\pi\xi} \sin\alpha \sin i \frac{\Delta T}{T} \frac{r_{\rm spot}^2}{R_1^2} P_{\rm orb}. \tag{4.11}$$

If we take the illustrative parameter values of $\xi = 0.04$, $\alpha = 45°$, $i = 40°$, $r_{\rm spot}/R_1 = 0.2$ (equivalent to a spot radius of 11.5° of arc on the stellar surface), $\Delta T/T = 0.15$, and $P_{\rm orb} = 8.7$ hours, we then find $\Delta\tau \sim$170 s, a value similar to those in our sample of $O-C$ curves.

4.3.3 Eclipses and Spot Occultations

An eclipse in a binary system consisting of two spherical stars of radii R_1 and R_2 and separation a will only occur if the inclination satisfies

$$i \gtrsim \cos^{-1}\left[\frac{R_1 + R_2}{a}\right] \tag{4.12}$$

Using the Eggleton (1983) analytic approximation for the size of the Roche lobe for a range of mass ratios of $0.3 \lesssim M_2/M_1 \lesssim 3$, we find that $(R_1 + R_2)/a$ ranges from 0.69 to 0.77, corresponding to a range of minimum inclination angles of 40° to 46°. We take a typical minimum inclination angle to observe an eclipse of $i_{\rm min} \simeq 41°$, corresponding to a mass ratio of unity.

This model only produces the anti-correlated behavior between the $O-C$ curves of the primary and secondary eclipse if the spot is not occulted by the companion star. If the spot is not occulted when it is located at longitude $\ell = 0$, then it will not be occulted when it is at any other longitude. If the radii of the star with the spot and the second star are R_1 and R_2 respectively, then we can derive the following

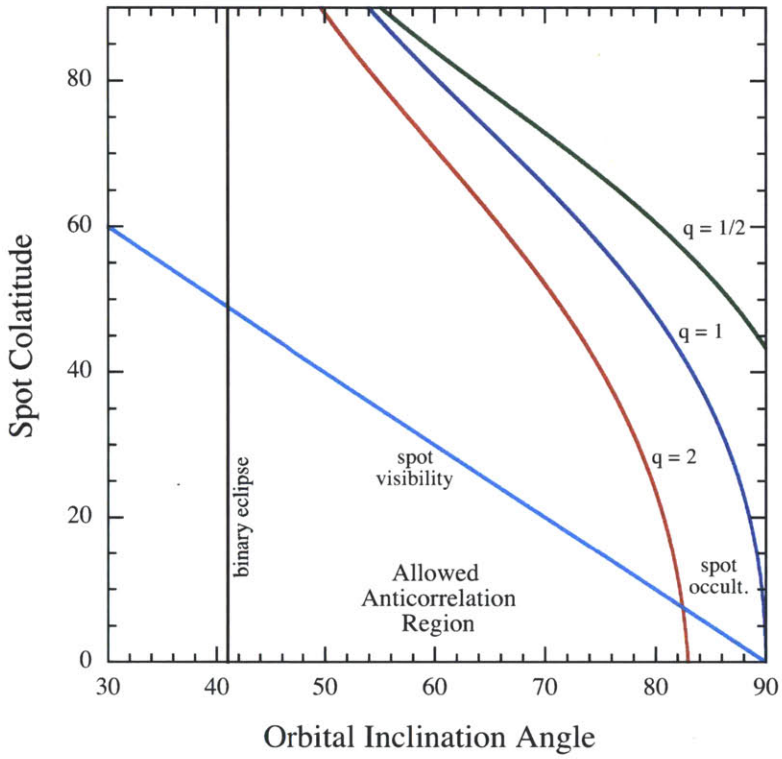

Figure 4-1: Geometric requirements for the observer to be able to see a starspot around an entire orbit of an eclipsing binary. The allowed region lies to the right of the vertical line (required for eclipses) and below the other curves. All angles are in degrees. The quantity q is defined as the mass ratio M_2/M_1.

condition on the inclination angle to avoid occultation of the spot at $\ell = 0$

$$\alpha < \sin^{-1}\left[\frac{a}{R_1}\cos i - \frac{R_2}{R_1}\right] + i \tag{4.13}$$

A plot of the constraints on the inclination angle and the spot colatitude is shown in Figure 4-1. The spot colatitude is plotted on the y axis and the inclination angle on the x axis. Viable regions in this parameter space lie to the right of the vertical line at 41°, below the spot visibility line given by the requirement that $\alpha + i < 90°$, and below the curves given by Equation (4.13).

4.4 Light Curve Simulations

In order to verify some of the approximations used for our model, the *Phoebe* binary light curve emulator was used to model a contact binary system where either one cool or one hot spot may be present on one star (Prša & Zwitter 2005). The *Kepler* contact binary KIC 3437800, whose $O - C$ curves exhibit anti-correlated behavior though it is not included in the present sample of 32 systems, served as a representative model. A *Phoebe* fit was done on the folded light curve, yielding the parameters $P_{\rm orb} = 8.7$ hours; $i = 40°$, $T_{\rm eff} = 6185$ K, and $q = M_2/M_1 = 0.62$ that would specify the baseline no-spot model. Orbital light curves were then simulated with a hot or cold spot placed at one of a variety of locations on the surface of the primary star. For this particular example, the spot was positioned at $\alpha = 45°$, $\ell = 90°$, was given a radius of 10° on the surface of the primary, and had a temperature that was elevated by 15% over the local $T_{\rm eff}$ of the star. The difference between the light curves of the model with the spot and the model without the spot is shown in Figure 4-2.

4.4.1 Limb Darkening

This difference curve is not exactly a pure sine function, a result that can understood in terms of limb darkening. We can modify Equation (4.4) with a simple linear limb darkening law such that

$$F_{\rm spot} \propto \cos\theta\,[1 - u(1 - \cos\theta)] \tag{4.14}$$

where $\cos\theta$ represents the dot product between the direction to the observer and the spot vector with respect to the center of its host star, and u is the linear limb-darkening coefficient. Substituting in the expression for the dot product, we can write

the above expression as

$$\begin{aligned} \Delta F_{\rm spot} &= A + b(1 - u + 2au)\cos(\omega t + \ell) + ub^2\cos^2(\omega t + \ell) \qquad (4.15) \\ A &= \text{DC offset} \\ a &= \cos\alpha\cos i \\ b &= \sin\alpha\sin i \end{aligned}$$

which is an equivalent expression to Equation (4.4), except for the addition of a $\cos^2$ term which accounts for limb darkening. A best-fit curve of the form given by Equation (4.15) was calculated and plotted superposed to the *Phoebe* simulated data in Figure 4-2.

In addition, *Phoebe* model light curves were computed for cases with the spot at a colatitude of $\alpha = 45°$ and centered at each of a set of longitudes covering the range $0° \leq \ell \leq 360°$. The times of the two eclipses and two out-of-eclipse maxima were found using the same interpolation method used for the actual *Kepler* data. The resulting $O-C$ curves are shown in Figure 4-3. The curves for each of the two eclipses exhibit anti-correlated behavior, as well as the curves for the two maxima. It is also important to note that they are not pure sine curves as expected from our simple model. This non-sinusoidal behavior may be due to the effect of limb darkening.

We rederived the analytic expressions for the phase shifts, as given in Equations (4.7) and (4.8), now accounting for limb darkening. The results were analogous to the original expressions, except that the $\sin\ell$ term in Equation (4.7) is multiplied by a factor of $(1 \pm \chi\cos\ell)$ while the $\cos\ell$ term in Equation (4.8) is multiplied by a factor $(1 \pm \chi\sin\ell)$, and χ is a geometry-dependent number of order $1/3 - 1/2$. Therefore, even after including limb darkening, the $O-C$ curves for the primary and secondary eclipses, as well as for the two maxima, are still anti-correlated in the sense that their values always have opposite signs, though the magnitudes are not quite equal. The *Phoebe* simulated $O - C$ data were fitted using the functions of ℓ given in Equations. (4.7) and (4.8), multiplied by the extra factor discussed above. The free parameter χ was found to be consistent with 0.45 ± 0.04 for all four curves. The

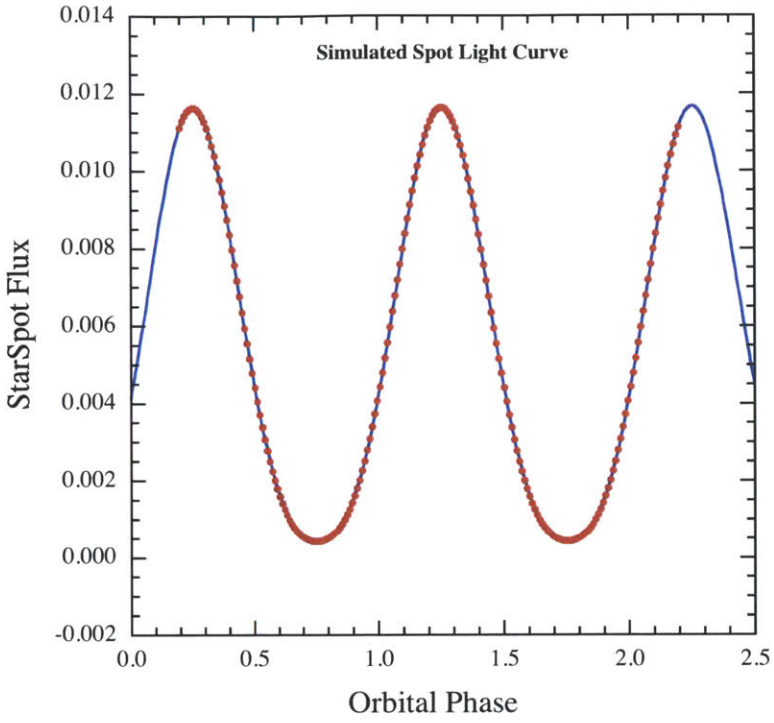

Figure 4-2: *Phoebe* generated light curve of a single hot spot. The red points are the relative flux coming from a hot spot as a function of the orbital phase. The blue curve is a model fit to Equation (4.15) in the text with ℓ set to 90°.

fitted curves are shown superposed in Figure 4-3.

4.5 Longer Period Binaries

It is interesting to wonder to what degree similar effects, especially anti-correlations between the $O-C$ curves for the primary and secondary eclipses, would be observable in longer period binaries. For longer orbital periods, the eclipse duration is given in terms of orbital cycles by

$$\frac{\Delta\theta_{\rm ecl}}{2\pi} = \frac{1}{\pi}\sin^{-1}\left[\frac{(R_1+R_2)}{a}\right] \simeq \frac{(R_1+R_2)}{\pi a} \tag{4.16}$$

assuming $R_1 \sim R_2 \ll a$. The eclipse profiles are approximated as in Equation (4.5) by taking $\mathcal{B} = -B\cos N\omega t$ for times t near those for which $\omega t = 0$ and $\omega t = \pi$. Here

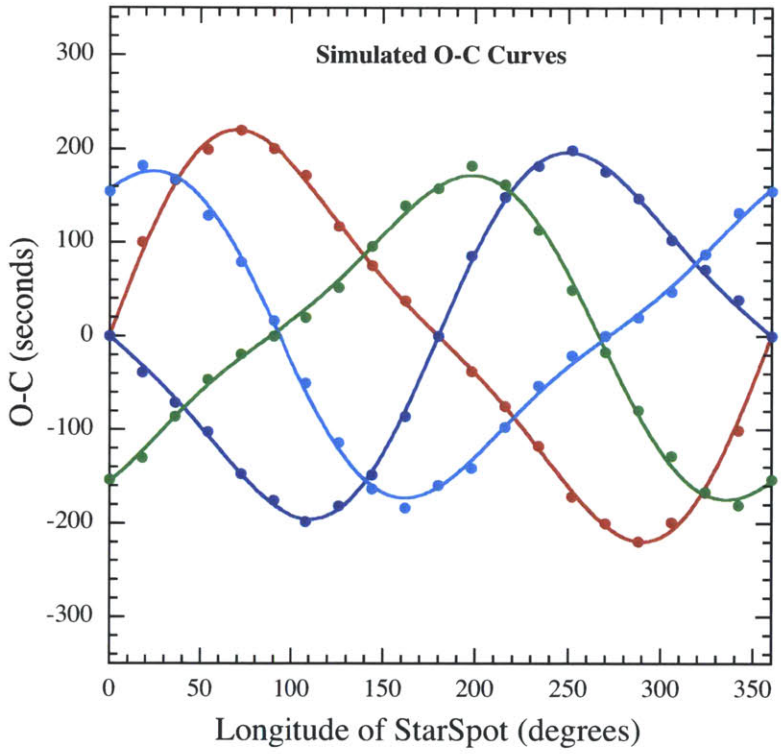

Figure 4-3: *Phoebe* generated $O-C$ curves for the binary system described in Figure 4-2, and modeled after KIC 3437800. The red and blue points are for the primary and secondary eclipses, respectively, while the green and cyan points are for the out-of-eclipse maxima. The smooth curves are fits to a simple spot model, modified by limb darkening.

N would be given by

$$N \simeq \frac{\pi}{\Delta\theta_{\rm ecl}} \simeq \frac{\pi a}{2(R_1 + R_2)} \tag{4.17}$$

We previously had taken $N = 2$ to represent a contact binary. For stars of a fixed, typical, unevolved size, this equation gives that $N \propto a \propto P_{\rm orb}^{2/3}$. We can recalculate the $O - C$ shifts in terms of N, resulting in

$$\Delta\tau \propto \frac{P_{\rm orb}}{N^2} \propto P_{\rm orb}^{-1/3} \tag{4.18}$$

If we consider a binary with a 30-day period, which is approximately two orders of magnitude longer than that of a typical contact binary, the spot-induced $O - C$ variations would be a factor of five less than those in a contact binary comprising similar stars and having similar spots.

In addition to this decrease in amplitude, several other effects also tend to reduce the observability of anti-correlated behavior in the $O - C$ curves of longer period binaries. For example, eclipses will only be seen in general for inclinations nearer to 90°. For larger inclination angles, starspots must be located nearer to the poles of the stars (see Figure 4-1) to avoid being occulted during the eclipses. Not only will the unocculted region be smaller, but also spots may be less likely to occur near a stellar pole. In addition, it is possible that contact binaries are more likely to have large spots and that any spots on them tend to be larger than the spots on the stars in longer period binaries. Finally, in order for the present starspot model to be effective in producing anti-correlated $O - C$ curves, the stars in the binary would be required to rotate nearly synchronously with the orbit, which is less likely to occur with increasing orbital period.

4.6 Multiple Starspots

Another important question about our simple model may be regarding the effects of the presence of more than one starspot. The result is simply a sum of terms

as given in Equation (4.7) but with a distributions of spot parameters, including different stellar longitudes. For the case where a single spot of a given area and temperature decrement is divided into n smaller spots of the same *total* area, and assigned a random distribution of ℓ values, the net result will be a simple decrease in the amplitude of the resultant $O-C$ curve by roughly $\sqrt{n}$. Thus, even if there are, e.g., 10 smaller spots present on one star, the amplitude of the shifts in eclipse timing are likely to be reduced by only a factor of a few. If, by contrast, the number of spots increases to n, but their sizes and temperature decrements remain unchanged, then the amplitude of the $O-C$ curve *increases* by $\sqrt{n}$. In either case, these collections of spots still have to migrate in a semi-coherent way, if quasi-periodic behaviors in the $O-C$ curves are to be observed.

4.7 Starspot Migration Periods

The quasi-periodic behavior of the $O-C$ curves may be informative about the surface differential rotation of the stellar components in our sample of binaries. We consider the following differential rotation law

$$P_\alpha = \frac{P_{\rm orb}}{(1 - k\cos^2\alpha)} \tag{4.19}$$

where α is the colatitude of the spot and P_α is the rotation period at colatitude α (Kalimeris et al. 2002; Hall & Busby 1990). The migration period $P_{\rm mig}$ is then

$$P_{\rm mig} = \frac{P_{\rm orb}^2}{(P_\alpha - P_{\rm orb})} \simeq \frac{P_{\rm orb}}{k\cos^2\alpha} \tag{4.20}$$

where the right hand approximation is based on the assumption that $k \ll 1$. If the 50 to 200 day time scales of the $O-C$ variations we observe in our sample are interpreted as migration periods, the values of k must be in the range 0.003 to 0.013, in good agreement with values cited by Kalimeris et al. (2002) and Hall & Busby (1990).

4.8 $O - C$ Behavior on Longer Timescales

As previously discussed, the $O - C$ curves for some systems exhibit positively correlated behavior on longer timescales. In an effort to enhance the shorter timescale anti-correlated variations due to the presence of starspots or eliminate them to look at longer timescale trends, we took the sum of the two $O - C$ curves for the primary and secondary eclipses, divided by a factor of 2, as well as the difference of the curves, also divided by 2. These sum and difference curves are particularly illuminating for systems that exhibit negatively correlated behavior on shorter timescales due to starspots, but positively correlated behavior on longer timescales, possibly due to physical changes in the orbital period.

An example of such a system is KIC 8956957, whose $O - C$ curves can be seen in a middle panel of Figure 3-4. The curves for this object are relatively flat on longer timescales but have many quasi-periodic short timescale variations. The summed average of the curves, which is shown in the top panel of Figure 4-4, indicates very little residual structure of interest. In contrast however, the difference of the curves, shown in the bottom panel of the figure, clearly enhances the quasi-periodic behavior.

Another example system is KIC 1873918, whose $O - C$ curves can be seen in the top panel of Figure 3-2. The curves for this object exhibit anti-correlated behavior in their shorter timescale quasi-periodic variations, but exhibit a positively correlated quadratic trend on longer timescales. In this case, the summed average of the curves, which is shown in the top panel of Figure 4-5, illustrates this long-term behavior, while the difference of the curves emphasizes the anti-correlated shorter timescale variations.

A fit to the long-term behavior of KIC 1873918, shown as a superimposed curve in the same figure, was calculated for the Roemer delay and the physical delay, both due to the presence of a third star (Rappaport et al. 2013). The parameters of the fit were: $P_{\rm orb} \simeq 854$ days, eccentricity $e \simeq 0.63$, longitude of periastron $\omega \simeq 251°$, Roemer amplitude $\simeq 280$ seconds, and mass function $\simeq 0.032\, M_{\odot}$.

These summed average and difference curves were produced for all the binaries in

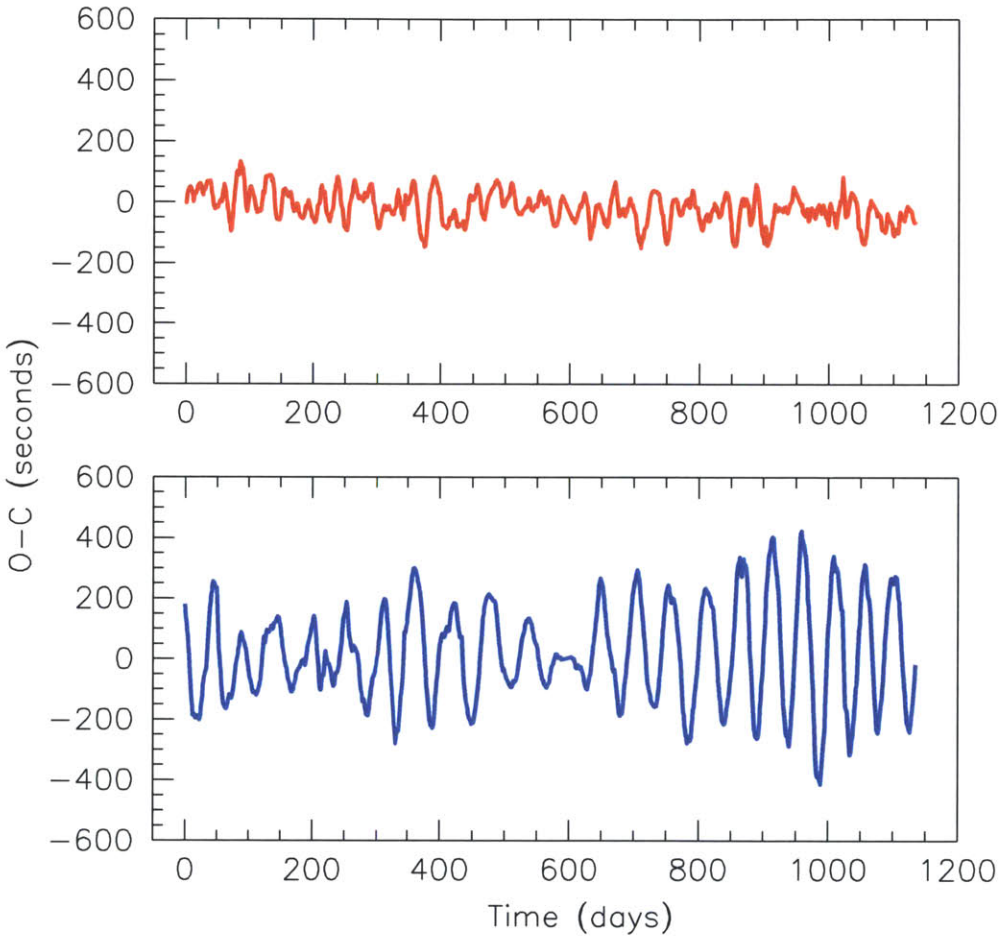

Figure 4-4: The sum (top panel) and difference (bottom panel) of the $O - C$ curves (divided by 2) for the primary and secondary eclipses of KIC 8956957, respectively. The summing of the curves eliminates the shorter timescale anti-correlated variations and results in a relatively quiet signal. On the other hand, taking the difference between the curves enhances these shorter timescale variations.

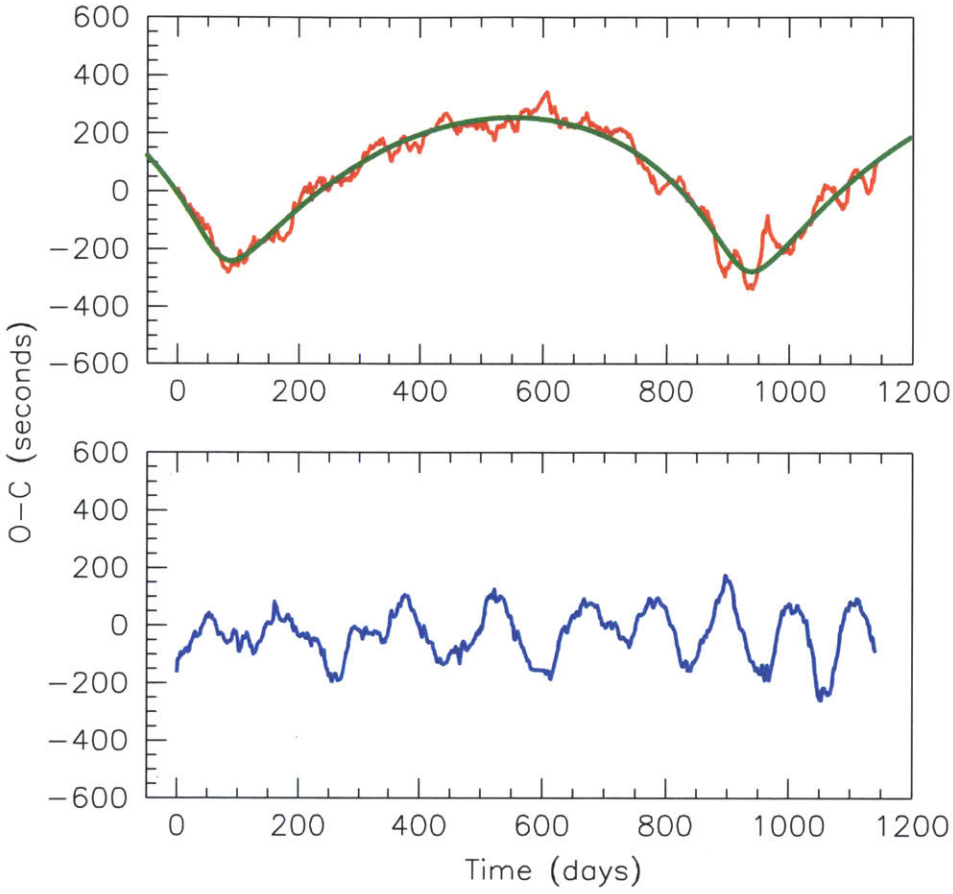

Figure 4-5: The sum (top panel) and difference (bottom panel) of the $O - C$ curves (divided by 2) for the primary and secondary eclipses of KIC 1873918, respectively. The summing of the curves eliminates the shorter timescale anti-correlated variations and results in a curve that shows the correlated longer timescale trend. The solid green curve on the top panel represents an orbital fit to the $O - C$ curve for the Roemer delay and the physical delay, both due to the presence of a third star.

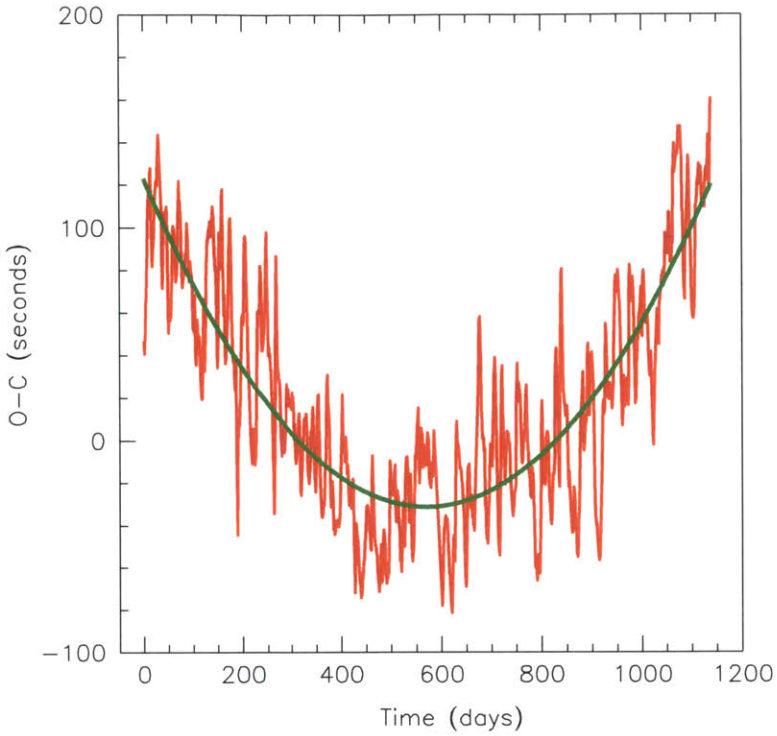

Figure 4-6: The summed average of the $O - C$ curves for the primary and secondary eclipses of KIC 9020289, shown in red. The solid green curve represents a fit to the quadratic long-term behavior of the summed curve. This fit has the quadratic term of $\dot{P}_{\rm orb} = 0.55 \pm 0.010 \times 10^{-8}$ days/day.

our selected sample in order to examine them for possible evidence of a third body. We found six systems (KIC 2715007, 4937350, 7691553, 9020289, 9097798, and 9821923) which clearly exhibit long-term quadratic trends, corresponding to approximately constant rates of change in the orbital periods of the binaries. Fits to the long-term trends of these curves gave quadratic terms of typical value of $\dot{P}_{\rm orb} \simeq 10^{-8}$ days/day, or $P_{\rm orb}/\dot{P}_{\rm orb} \simeq 0.1$ Myr. The summed average curve for KIC 9020289 is shown in Figure 4-6 with a fit to the long-term quadratic trend.

The presence of such long-term quadratic trends in the $O - C$ curves of contact binaries is not unusual. A previous study lists 42 systems that exhibit such behavior, calculating a mean value of $P_{\rm orb}/\dot{P}_{\rm orb} \simeq 2.7$ Myr for 12 contact binaries and 4.4 Myr for an additional 10 classified as "hot contact binaries" (Qian 2001a; 2001b). These values for the change in orbital period indicate much slower evolving periods than the

ones in our sample, but the sensity of that study is mostly due to the long historical baseline that was used (80 years vs. *Kepler*'s 4 year duration). Larger values of $\dot{P}_{\rm orb}$ in contact binaries have also been detected, such as LP UMa, with $P_{\rm orb}/\dot{P}_{\rm orb} \simeq 0.2$ Myr (Csizmadia, Bíró, & Borkovits 2003).

The long-term quadratic trend of the curve could be indicative the presence of a third body in an orbit about, or much longer than, the length of the *Kepler* data train. It is also possible that evolutionary effects could be a physical cause for these long-term changes in the binary orbital periods. Such effects could include mass transfer between the stellar components of the binaries (Lucy 1976; Webbink 1976; Webbink 2003), or angular momentum loss, driven by magnetic braking due to either the companion star (Mochnacki 1981), or the stellar winds (van't Veer 1979). Another possibility could be the simultaneous mass and angular momentum loss via stellar winds (van't Veer & Maceroni 1989).

Chapter 5

Conclusions

Kalimeris et al. (2002) and earlier works showed that photometric perturbations, and, in particular, starspots may affect measured $O-C$ times, and that those perturbations are not properly interpreted in terms of orbital period changes. They noted that spot migration could produce (quasi)periodic effects in the O-C curves.

In this work, we have substantially extended these earlier results. We have used (a) the *Kepler* data base for binary stars, and (b) an analytic model to provide good insight into the timing effects of starspots on the $O-C$ curves. In particular, we (i) identified a sample of *Kepler* target short-period binaries (i.e., $P_{\rm orb} \lesssim 1$ day) that appear to manifest the effects of a single spot or a small number of spots on their $O-C$ curves; these quite often have the form of a random-walk or quasiperiodic behavior, with typical amplitudes of $\sim \pm$ 300 s. Most of these $O-C$ curves also exhibit a very pronounced anticorrelation between the primary and secondary eclipses. (ii) We developed a simple idealized model that illustrates the major effects that starspots have on measured eclipse times. In particular (iii) we showed that a spot will, in general, affect the times of primary minimum and secondary minimum differently, with the predominant effect being an anticorrelated behavior between the two, provided that the spot is visible around much of the binary orbit. (iv) We also showed that a spot can equally well affect the times of the two maxima in each orbital cycle, and that the effects on the two maxima should be different, typically including anticorrelated behavior between them and a 90° phase shift with respect to the eclipse minima.

(v) All of the same types of timing behavior are expected for close binaries that do not eclipse at all, i.e., so-called "ELV" binaries, and in fact, 8 of our sample of 32 systems that we have highlighted are in this latter category. (vi) We have found that a few of the selected contact binaries showed positively correlated variations in the $O - C$ curves for their primary and secondary eclipses on long time scales as well as the anticorrelated variations that are most evident on shorter time scales. We then demonstrated (vii) that sum and difference $O - C$ curves between the primary and secondary eclipses are useful in distinguishing between the two types of variations. (viii) We used this latter technique (i.e., of summing the two $O - C$ curves of the primary and secondary eclipses) to better isolate the effects of a possible third body in the system. In the process we found a likely Roemer delay curve for one of the systems, as well as convincing evidence for a long-term quadratic trend in six other systems. (ix) Finally, we found that the $O - C$ difference curves often appear to be dominated by 50 to 200 day quasiperiodicities that we interpret in terms of the migration of spots relative to the frame rotating with the orbital motion.

Bibliography

[1] Algol, E. On detecting terrestrial planets with timing of giant planet transits. *Monthly Notices of the Royal Astronomical Society, 359*(2): 567, 2005.

[2] Barnes, J. R., Lister, T. A., Hilditch, R. W., & Collier Cameron, A. *Monthly Notices of the Royal Astronomical Society, 348*: 1321, 2004.

[3] Batalha, N.M., Rowe, J.F., Bryson, S.T., et al. *The Astrophysical Journal, Supplement, 204*: 24, 2013.

[4] Bhattacharyya, S. X-ray views of neutron star low-mass X-ray binaries. *Current Science, 97*: 804, 2009.

[5] Borkovits, T. et al. On the detectability of long period perturbations in close hierarchical triple stellar systems. *Astronomy & Astrophysics, 398*: 1091, 2003.

[6] Borkovits, T. et al. Tidal and rotational effects in the perturbations of hierarchical triple stellar systems. II. Eccentric systems - the case of AS Camelopardalis. *Astronomy & Astrophysics, 473*(1): 191, 2007.

[7] Borucki, W. J., et al *Science, 327*: 977, 2010.

[8] Brown, E. W. The stellar problem of three bodies. II. The equations of motion with a simplified solution. *Monthly Notices of the Royal Astronomical Society, 97*: 62, 1936.

[9] Caldwell, D.A. *The Astrophysical Journal, Letters, 713*: L92, 2010.

[10] Csizmadia, Sz., Bíró, I.B., & Borkovits, T. *Astronomy & Astrophysics, 403*: 637, 2003.

[11] Csizmadia, Sz., Patkós, L., Moór, A., & Könyves, V. *Astronomy & Astrophysics, 417*: 745, 2004.

[12] Csizmadia, Sz., Kövári, Z., Klagyivik, P. *Astrophysics & Space Science, 304*: 355, 2006.

[13] Csizmadia, Sz. & Klagyivik, P. *Astronomy & Astrophysics, 426*: 1001, 2004.

[14] Eggleton, P. P. Approximations to the radii of Roche lobes. *The Astrophysical Journal, 268*: 368, 1983.

[15] Eggleton, P. P. *Evolutionary Processes in Binary and Multiple Stars.* ISBN 0521855578. Cambridge, UK: Cambridge University Press, 2006.

[16] Fabrycky, D. & Tremaine, S. *The Astrophysical Journal, 669*: 1298, 2007.

[17] Gazeas K. & Stepień K. *Monthly Notices of the Royal Astronomical Society, 390*: 1577, 2008.

[18] Gimenez, A., & Garcia-Pelayo, J.M. *The Astrophysical Journal, Supplement, 92*: 203, 1983.

[19] Hall, D.S. & Busby, M.R. Active Close Binaries, ed. C. Ibanoglu (Dordrecht: Kluwer), 377, 1990.

[20] Harrington. R. S. Dynamical evolution of triple stars *Astronomical Journal, 73*: 109, 1968.

[21] Harrington. R. S. The Stellar Three-Body Problem. *Celestial Mechanics, 1*(2): 200, 1969.

[22] Hendry, P.D. & Mochnacki, S.W. *The Astrophysical Journal, 531*: 467, 2000.

[23] Kalimeris, A., Rovithis-Livaniou, H., & Rovithis, P. *Astronomy & Astrophysics, 387*: 969, 2002.

[24] Kähler, H. *Astronomy & Astrophysics, 395*: 899, 2002.

[25] Kähler, H. *Astronomy & Astrophysics, 414*: 317, 2004.

[26] Kiseleva, L. G., Eggleton, P. P., & Mikkola, S. *Monthly Notices of the Royal Astronomical Society, 300*: 292, 1998.

[27] Koch, D.G., et al. *The Astrophysical Journal, Letters 713*: L79, 2010.

[28] Kozai, Y. *The Astronomical Journal, 67*: 591, 1962.

[29] Li, L., Han, Z., & Zhang, F. *Monthly Notices of the Royal Astronomical Society, 351*: 137, 2004.

[30] Li, L., Zhang, F., Han, Z., Jiang, D., & Jiang, T. *Monthly Notices of the Royal Astronomical Society, 387*: 97, 2008.

[31] Lucy, L. B. *The Astrophysical Journal, 151*: 1123, 1968.

[32] Lucy, L. B. *The Astrophysical Journal, 205, 208*: 1976.

[33] Maceroni, C., Vilhu, O., van't Veer, F., & van Hamme, W. *Astronomy & Astrophysics, 288*: 529, 1994.

[34] Maceroni, C. & van't Veer, F. *Astronomy & Astrophysics, 311*: 523, 1996.

[35] Matijevič, G., Prša, A., Orosz, J.A., Welsh, W.F., Bloemen, S., Barclay, T. *The Astronomical Journal, 143*: 123, 2012.

[36] Mochnacki, S.W. *The Astrophysical Journal, 245*: 650, 1981.

[37] Qian, S. *Monthly Notices of the Royal Astronomical Society, 328*: 635, 2001a/

[38] Qian, S. *Monthly Notices of the Royal Astronomical Society, 328*: 914, 2001b.

[39] Paczyński, B., Szczygieł, D. M., Pilecki, B.; Pojmański, G. *Monthly Notices of the Royal Astronomical Society, 368*: 1311, 2006.

[40] Prša, A., & Zwitter, T. *The Astrophysical Journal, 628*: 426, 2005.

[41] Rappaport, S., Deck, K., Levine, A., Borkovits, T., Carter, J., El Mellah, I., Sanchis-Ojeda, R., & Kalomeni, B. Triple-star Candidates among the Kepler Binaries. *The Astrophysical Journal, 768*(1): 33, May 2013.

[42] Robertson, J. A., & Eggleton, P. P. *Monthly Notices of the Royal Astronomical Society, 179*: 359, 1977.

[43] Ole Christensen Roemer. Démonstration touchant le mouvement de la lumière trouvé par M. Roemer de l'Académie des Sciences. emphJournal des Scavans: 276, 1676.

[44] Rucinski, S. M. *The Astronomical Journal, 116*: 2998, 1998.

[45] Senavci, T., Hussain, G. A. J., O'Neal, D., & Barnes, J. R. *Astronomy & Astrophysics, 529*: 11, 2011.

[46] Slawson, R., et al. *The Astronomical Journal, 142*: 160, 2011.

[47] Smith, J. C. et al. Kepler Presearch Data Conditioning II - A Bayesian Approach to Systematic Error Correction. *Publications of the Astronomical Society of the Pacific, 124*(919): 1000, 2012.

[48] Soderhjelm, S. The three-body problem and eclipsing binaries - Application to algol and lambda Tauri. *Astronomy & Astrophysics, 42*(2): 229, 1974.

[49] Soderhjelm, S. Studies of the stellar three-body problem. *Astronomy & Astrophysics, 107*(1): 54, 1982.

[50] Soderhjelm, S. Third-order and tidal effects in the stellar three-body problem. *Astronomy & Astrophysics, 141*(1): 232, 1984.

[51] Stepień, K. & Gazeas, K. *Annual Review of Astronomy and Astrophysics, 62*: 153, 2012.

[52] Stumpe, M. C. et al. Kepler Presearch Data Conditioning I - Architecture and Algorithms for Error Correction in Kepler Light Curves. *Publications of the Astronomical Society of the Pacific, 124*(919): 985, 2012.

[53] van't Veer, F.*Astronomy & Astrophysics, 80*: 287, 1979.

[54] van't Veer, F. & Maceroni, C. *Astronomy & Astrophysics, 220*: 128, 1989.

[55] Webbink, R. *The Astrophysical Journal, 209*: 829, 1976.

[56] Webbink, R.F. 3D Stellar Evolution. eds. S. Turcotte, S. C. Keller, & R. M. Cavallo. *Astronomical Society of the Pacific Conference Series, 293*: 76, 2003.

[57] Wilson, R. E.. *Publications of the Astronomical Society of the Pacific PASP, 106*: 921, 1994.

[58] Yakut, K. & Eggleton, P. P. *The Astrophysical Journal, 629*: 1055, 2005.